Polyvinylpyrrolidone (PVP) in nanoparticle synthesis

Kallum M. Koczkur, Stefanos Mourdikoudis, Lakshminarayana Polavarapu, Sara E. Skrabalak

Polyvinylpyrrolidone (PVP) in nanoparticle synthesis

Kallum M. Koczkur[a,*], Stefanos Mourdikoudis[b,c,*], Lakshminarayana Polavarapu[d,e,*] and Sara E. Skrabalak[a,*]

[a] Indiana University, Department of Chemistry, 800 E. Kirkwood Ave., Bloomington, IN 47405-7102, USA

[b] Sorbonne Universités, UPMC Univ Paris 06, UMR 8233, MONARIS, F-75005, Paris, France

[c] CNRS, UMR 8233, MONARIS, F-75005, Paris, France

[d] Photonics and Optoelectronics Group, Department of Physics and CeNS, Ludwig-Maximilians-Universität München, Munich, Germany

[e] Nanosystems Initiative Munich (NIM), Munich, Germany

ABSTRACT: Colloidal synthesis offers a route to nanoparticles (NPs) with controlled composition and structural features. This Perspective describes the use of polyvinylpyrrolidone (PVP) to obtain such nanostructures. PVP can serve as a surface stabilizer, growth modifier, nanoparticle dispersant, and reducing agent. As shown with examples, its role depends on the synthetic conditions. This dependence arises from the amphiphilic nature of PVP along with the molecular weight of the selected PVP. These characteristics can affect nanoparticle growth and morphology by providing solubility in diverse solvents, selective surface stabilization, and even access to kinetically controlled growth conditions. This Perspective includes discussions of the properties of PVP-capped NPs for surface enhanced Raman spectroscopy (SERS), assembly, catalysis, and more. The contribution of PVP to these properties as well as its removal is considered. Ultimately, the NPs accessed through the use of PVP in colloidal syntheses are opening new applications, and the concluding guidelines provided herein should enable new nanostructures to be accessed facilely.

1. Introduction

Wet-chemical pathways to nanoparticles (NPs) have progressed to provide monodisperse samples of many material classes. Yet reaction parameters often remain unexplored but contribute to important structural features of NPs. For example, crystallite size often correlates with improved or new properties for metal, metal oxide, and metal chalcogenide NPs. Such properties include size-dependent optical, catalytic, and magnetic behaviour. However, the acquisition of NPs with desired characteristics requires the use of reagents that bind onto the surfaces of particles in a way that the expected properties are maintained or enhanced. In addition, the role of each reagent in the growth process has to be understood thoroughly in order to develop synthetic protocols to new advanced nanostructures.

We have reviewed chemical routes to NPs from several perspectives: shape-control,[1,2] growth mechanism,[3] engineering of remarkable properties,[4] and reagents such as common ligands[5] and oleylamine.[6] Given the interest in nanomaterial synthesis, various reviews and book chapters are provided by other groups as well.[7,8,9] Here, the first comprehensive review of polyvinylpyrrolidone (PVP) in colloidal NP synthesis is provided. By surveying the conditions that produce metals, metal oxides, and metal chalcogenides with defined structural features, the contributions of PVP to nanostructure formation emerge. Significantly, PVP can serve as a surface stabilizer, growth modifier, nanoparticle dispersant, and reducing agent depending on the specific synthetic conditions and material system.

PVP is a bulky, non-toxic,[10] non-ionic[11] polymer with C=O, C-N and CH_2 functional groups[12] that is widely used in NP synthesis. The PVP molecule contains a strongly hydrophilic component (the pyrrolidone moiety) and a considerable hydrophobic group (the alkyl group, see Scheme 1a and b).[13] Water and many non-aqueous liquids are excellent solvents for PVP, as a result of the highly polar amide group within the pyrrolidone ring and apolar methylene and methine groups in the ring and along its backbone.[14] PVP is a great stabilizer, preventing the aggregation of NPs via the repulsive forces that arise from its hydrophobic carbon chains that extend into solvents and interact with each other (steric hindrance effect).[15] In some cases, the obtained interparticle distances are so elongated that PVP can be considered a 'dispersant'. Moreover, the length of PVP plays an important role in the stabilization of NPs.[16] This conclusion is based on a recent report on atomistic molecular dynamics (MD) simulations of Ag NPs capped with PVP oligomers of varying

chain length which revealed that longer chains provide enhanced stability through effective protection of Ag core (Scheme 1c).[16] PVP is often a shape-control agent, promoting growth of specific crystal faces while hindering others.[17] For example, PVP strongly binds to the {100} facets of Ag when dispersed in polyols, allowing growth along <111> directions to obtain Ag nanowires (NWs; Scheme 1d), which was also confirmed through density functional theory (DFT) methods by Saidi *et al.*[18] The conditions which enable shape control in PVP systems are discussed thoroughly as a function of material class. PVP as a mild reductant is also described as the ends of this molecule are terminated in hydroxyl groups.[19] An important feature of PVP is the existence of carbonyl oxygens which can hydrogen bond solvent molecules. PVP is a remarkably stable polymer, with inert physicochemical properties over a broad range of pH values.[20]

FTIR spectroscopy is often used to study the interaction of PVP with NP surfaces. Fig. 1 shows a FTIR spectrum of PVP and provides the assignment of the principal FTIR bands.[21] The amount of PVP on NP surfaces can be characterized by thermogravimetric and derivative thermogravimetric analysis (TGA and DTG).[22,23,24] Fig. 2 shows the TGA and DTG curves for PVP and PVP-capped Ag nanoplates in air and N_2. PVP alone decomposes around 400 ^{o}C in air, although slight variations have been reported.[25,26] When bound to Ag NPs, decomposition temperatures between 200 and 400 ^{o}C have been reported in the literature at different experimental conditions.[22,23,24] Finally, PVP is available with different molecular weights, and parameters such as viscosity in aqueous solution, decomposition temperature, and redox potential depend on this property.[27]

In the next sections, the roles of PVP in the synthesis of different nanostructures are highlighted as a function of material class. Section 2 presents metallic and bimetallic NPs (mainly Ag, Au, Pd, Pt, and their combinations). Metal oxide nanomaterials are described in Section 3 and Section 4 analyzes the synthesis of metal chalcogenide nanomaterials. Finally, Section 5 discusses the use of PVP in other nanomaterial systems.

2. PVP in the synthesis of metallic NPs

PVP is widely used as a stabilizing and shape-directing agent in the polyol synthesis of metallic NPs. Examples of these NPs include plasmonic elements (Ag, Au, Cu),[28,29,30,31,32,33,34] catalytic elements (Pd, Pt),[35,36,37,38] magnetic elements (Co, Ni)[39,40] and bimetallic compositions (Au-M, Pt-M).[41,42,43,44] For noble metals, the metal-PVP interaction occurs through the carbonyl group and nitrogen atom of the pyrrolidone ring based off of X-ray photoelectron spectroscopy (XPS), TGA, Fourier transform Raman (FT-Raman), and FTIR spectroscopy studies.[22,45,46] A recent computational study of PVP adsorbed on Ag nanocrystals using DFT suggests that the surface-selective interaction of PVP with the lowest-energy crystal facets, {100} and {111}, occurs through van der Waals (vdW) attraction and direct binding.[47] Interest in shape-controlled metallic NPs has steadily increased since a seminal paper by Sun and Xia detailed the synthesis of Ag nanocubes.[48] PVP played a vital role in the synthesis through stabilization of the {100} facets, which allowed cubes to grow in comparison to multiply twinned particles (MTP) bound by the more stable {111} facets when PVP is absent.[48] Numerous manuscripts have since reported shape-controlled NPs using PVP-assisted polyol syntheses.[1,49,50] The goal of this section is to highlight how the PVP-metal interaction affects the shape of particles, with a focus on noble metal NPs.

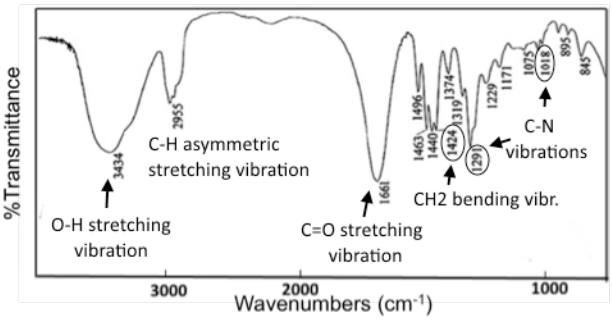

Fig. 1 FTIR spectrum of PVP. The main IR vibrational assignments are denoted inside the Figure with arrows.[21,51] (Figure reproduced and adapted with permission from ref. 21)

Silver nanostructures prepared with PVP. Ag has high thermal and electrical conductivity. These properties make Ag an important material for electronics, for example as contacts in circuit boards. Ag nanostructures also display size- and shape-dependent localized surface plasmon resonances (LSPRs) which enable new applications in nanomedicine,[52] photocatalysis,[53] and chemical sensing based on surface enhanced Raman spectroscopy (SERS)[54] and refractive index sensitivity.[55] PVP is instrumental toward achieving shape-control in Ag systems, with a variety of convex structures demonstrated. Examples include {100}-encased nanocubes, {111}-encased octahedra, and mixed faceted cuboctahedra, all from single-crystalline seeds.[48,49,56] Complementary to the report by Sun and Xia,[48] Yang and co-workers demonstrated monodisperse Ag nanocrystals from simultaneous addition of $AgNO_3$ and PVP into hot pentanediol (180 °C).[57] Nanocubes formed at the beginning of the reaction and were thought to be stabilized by PVP selectively adsorbing to {100} facets. Continued addition of $AgNO_3$ and PVP led to Ag octahedra after 2 hours. The authors concluded that the PVP may not completely control shape in this system as {111} facets could also be expressed.[57]

An important consideration in determining nanocrystal morphology is surface free energy.[49,58] Empirically, PVP appears to stabilize {100} Ag facets in polyols based on the preference for {100}-encased structures achieved in its presence.[1,47,49] Both experimental and theoretical work suggest that PVP lies flat on Ag surfaces and the higher binding energy of PVP to Ag {100} facets arises from vdW attraction and direct binding through the oxygen atom.[47] However, no quantitative study of PVP in metal nanocrystal growth was reported until recently.[56]

Xia and co-workers hypothesized that the morphology of Ag nanocubes could be altered by changing surface coverage through PVP concentration and molecular weight in solution. This hypothesis was tested by using Ag nanocubic seeds with edge lengths of 40 and 100 nm to facilitate Ag growth, with $AgNO_3$ being reduced in heated ethylene glycol (EG). The concentrations and molecular weights of PVP were varied from 1.0 to 0.1 mM for the 40 nm seeds and 2.5 to 0.3 mM for the 100 nm seeds; PVP55 (molecular weight ~ 55,000; note that molecular weights are denoted as "PVP$\frac{MW}{1000}$" hereafter) and PVP10 were used in both sets of experiments.[56] Aliquots from various times were analyzed for morphological changes.

SEM images of the Ag nanocrystals achieved at different concentrations and molecular weights using 40 nm cubic seeds are shown in Fig. 3.[56] In the case of PVP55, differences in Ag nanocrystal shape were observed as a function of PVP concentration as early as 5 minutes and are accentuated at longer times. Specifically, {100}-terminated Ag nanocubes are achieved at higher concentrations (1.0 mM) after 5 minutes (Fig. 3a). In contrast, truncation of the corners is observed within 5 minutes at lower concentrations (0.1 mM) (Fig. 3b). After 20 minutes, the Ag nanocubes have grown in size, with slight truncation at the corners to express {111} facets (Fig. 3c); however, the truncated cubes achieved at lower concentrations have grown to octahedra (Fig. 3d).

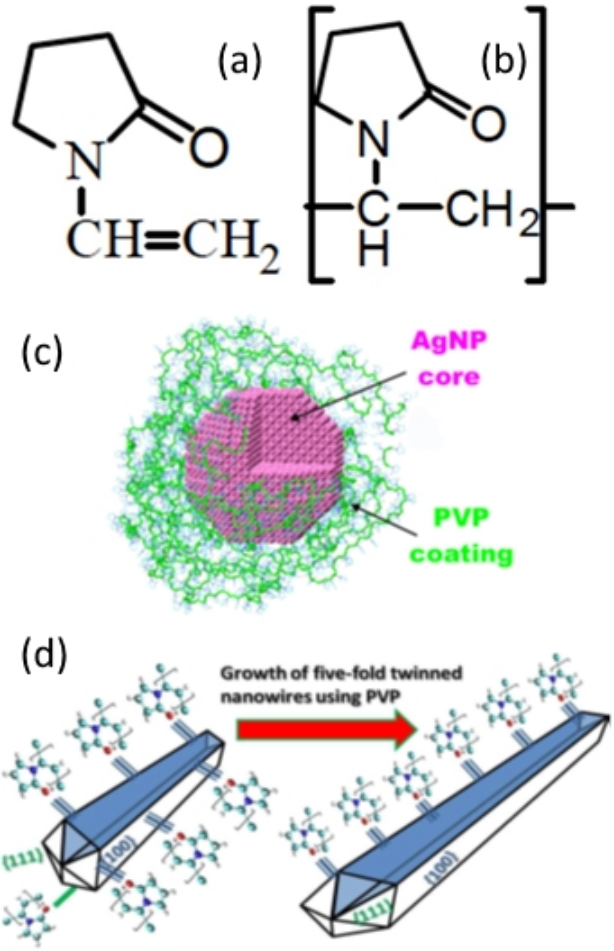

Scheme 1 (a) Molecular structure of the monomer N-vinylpyrrolidone and (b) the repeating unit of PVP.[13] (c) snapshot of MD simulations of a Ag NP interacting with PVP oligomers in the aqueous environment,[16] and (d) a schematic of the PVP-directed growth mechanism for Ag NWs (PVP binds strongly to the {100} facets to facilitate growth along <111> directions).[18] (Figures (c) and (d) were reprinted with permission from ref. 16 and 18 respectively)

This difference was attributed to the initial concentration of PVP in solution being high enough to maintain coverage density on the Ag seeds as they grew. Once the concentration of free PVP in solution drops below a critical level, passivation of the Ag cube surfaces can no longer be sustained and the surface free energy of {111} facets becomes similar to the surface free energy of the {100} facets. This situation allows the {111} facets to grow. UV-visible spectra of the Ag nanocrystals showed red-shifting of the major LSPR peak as the nanocrystals were enlarged.[56]

Interestingly, when PVP10 was used under similar reaction conditions, differences in the final nanocrystal shapes were observed. Specifically, the 40 nm cubic seeds can grow to 130 nm in edge length, with the cubic shape preserved at high PVP10 concentrations and long reaction times (Fig. 3e). Decreasing the PVP10 concentration results in the 40 nm cubic seeds growing into truncated octahedra. The authors summarized that PVP10 was more efficient at minimizing the surface free energy of Ag(100) when compared to PVP55, possibly due to PVP10 packing more efficiently on the surface of the Ag cubes on account of its smaller size. This interpretation was supported by surface coverage (ϕ) calculations that showed ϕ values of approximately 140 repeating units per nm^2 for PVP55 and approximately 30 repeating units per nm^2 for PVP10 when using 40 nm seeds.[56]

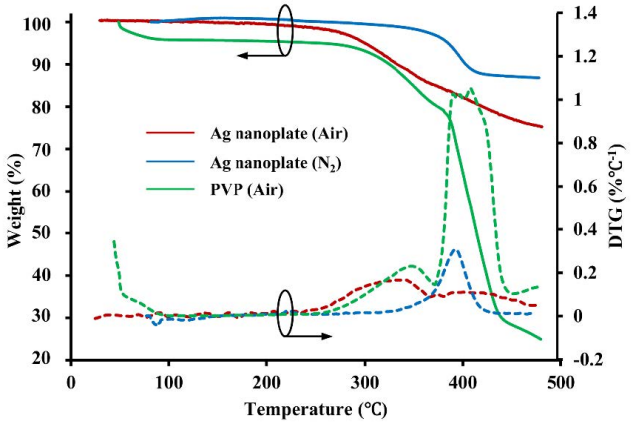

Fig. 2 TGA/DGA of PVP and PVP-capped Ag nanoplates in air and N_2.[23] (Figure reprinted with permission from ref. 23)

SERS studies of PVP55 adsorbed on the surfaces of Ag cubes[56] and octahedra are shown in Fig. 3g and indicate differences in the intensities of the PVP signals. The in-ring stretching modes, C-C stretching modes, and CH_2 rocking are all visible for PVP adsorbed on the cubes, whereas these modes are weak for PVP adsorbed on the octahedra. The largest difference was in the carbonyl stretching region where the peak for the nanocube sample is several times larger. When SERS spectra were collected for the cubes and octahedra modified with 1,4-benzenedithiol, the enhancement factors were both on the order of $1x10^5$, indicating that thiol adsorption is not facet dependent. The authors interpreted the differences in the SERS spectra of cubes and octahedra with PVP to the coverage density of PVP being much higher on the cubes.[56]

The ratio of {111} area ($A_{\{111\}}$) to {100} area ($A_{\{100\}}$) plotted as a function of time as Ag nanocrystals grow from 40 nm seeds are shown in Fig. 3h. Both concentrations of PVP10 yielded fairly constant ratios of $A_{\{111\}}/A_{\{100\}}$, the same with 1.0 mM PVP55. However, when 0.1 mM PVP55 was used, the facet ratio increased substantially from 10 to 20 minutes. These results are consistent with {111} facet growth resulting from insufficient PVP55 adsorbed to the {100} facets to maintain the lowered surface free energy. This investigation showed that the concentration and molecular weight of PVP

used were vital in determining the morphology of the nanocrystals.[56]

Additional shape-defined Ag nanostructures have been reported using polyol syntheses with PVP as a capping agent. For example, Ag NWs are heavily studied for applications in sensing and plasmonics and are prepared by various methods.[22,59,60,61,62,63,64,65] PVP-assisted polyol syntheses of Ag NWs began with work from Xia and co-workers, where $AgNO_3$ was reduced in EG with PVP55 and either Ag or Pt seeds present (Fig. 4a).[59,60] The growth originates from the seeds, which are decahedral in shape.[60,62] The 1-D growth is facilitated by addition of Ag to the {111} facets at the ends of the seeds, with the {100} facets that emerge during growth being passivated by PVP.[62] The surface protecting role of PVP, supported by XPS studies, is through the interaction of the carbonyl oxygen of the repeating unit and Ag surface atoms. The PVP/$AgNO_3$ ratio also contributes to shape as high ratios, 18 for example, yielded only Ag NPs. This observation suggests that PVP passivates all seed facets at high concentrations. In contrast, low ratios, 1.5 for example, led to wires that were longer and thicker as there was insufficient PVP in solution to maintain passivation of the {100} sides of the wires.[60]

Other anisotropic structures such as Ag nanoflags (Fig. 4b)[66] have been produced in the presence of PVP. In the case of Ag nanoflags, these structures form through a two-step process, with the first step being the synthesis of pentagonally twinned nanorods. They are synthesized from EG, $AgNO_3$, NaCl, and PVP40. The nanorods were collected by centrifugation and used as seeds, in a DMF solution, with $AgNO_3$ and PVP40. The flags are {111}-faceted, and the authors suggested that DMF as the solvent and reducing agent changes the preferential adsorption of PVP to {111} Ag facets rather than {100} facets when using EG as the solvent and source of reducing agent.[66] Different flag structures form depending on the ratio of $AgNO_3$ in the second step (denoted as $[AgNO_3]_{S2}$) compared to $AgNO_3$ used in the first step (denoted as $[AgNO_3]_{S1}$). For example, a $[AgNO_3]_{S2}/[AgNO_3]_{S1}$ ratio of 150 resulted in trapezoidal and triangular flags while a ratio of 400 resulted in tetrahedral flags.[66]

{100}-terminated Ag right bipyramids also form in polyol syntheses, using EG, $AgNO_3$, and PVP at a temperature of 160 °C, as seen in Fig. 4c.[67] The structures contain a (111) twin plane and are grown from singly twinned seeds which can be isolated by oxidative etching which removes MTPs. Central to this synthesis is the use of PVP as a {100}-selective capping agent.[67] By selectively stabilizing {100} facets of Ag, the PVP-Ag interaction will lower the surface free energy of the {100} facets relative to the {111} facets and grow nanocrystals that maximize the expression of {100} facets.[58] Right bipyramids of different sizes could be isolated at reaction times ranging from 2 ½ to 5 hours.[67]

Ag nanobeams also form by PVP-assisted polyol methods and have excellent current-carrying and resistivity properties.[68] The nanobeams were synthesized from $AgNO_3$, EG, NaBr, and PVP at a temperature of 148 °C and grew from singly twinned seeds.[68] SEM images of the Ag nanobeams indicate a rounded profile (Fig. 4d).[68] Interestingly, the synthesis of the nanobeams is similar to that of the right bipyramids,[67] just the concentrations of $AgNO_3$ and PVP are doubled. The authors suggested the nanobeams grew anisotropically as a result of kinetically controlled growth conditions.[68]

In summary, PVP is a versatile shape-directing and stabilizing agent for monodisperse Ag nanostructure syntheses. In EG, PVP stabilizes {100} Ag facets through interaction of the carbonyl groups of the repeating unit with metal surface. Xia and co-workers recently provided the first quantitative examination of the role PVP plays in the polyol synthesis of shape-controlled Ag nanocrystals. They found that the molecular weight and concentration of PVP was vital in determining the morphology of the Ag nanocrystals. The Ag nanostructures

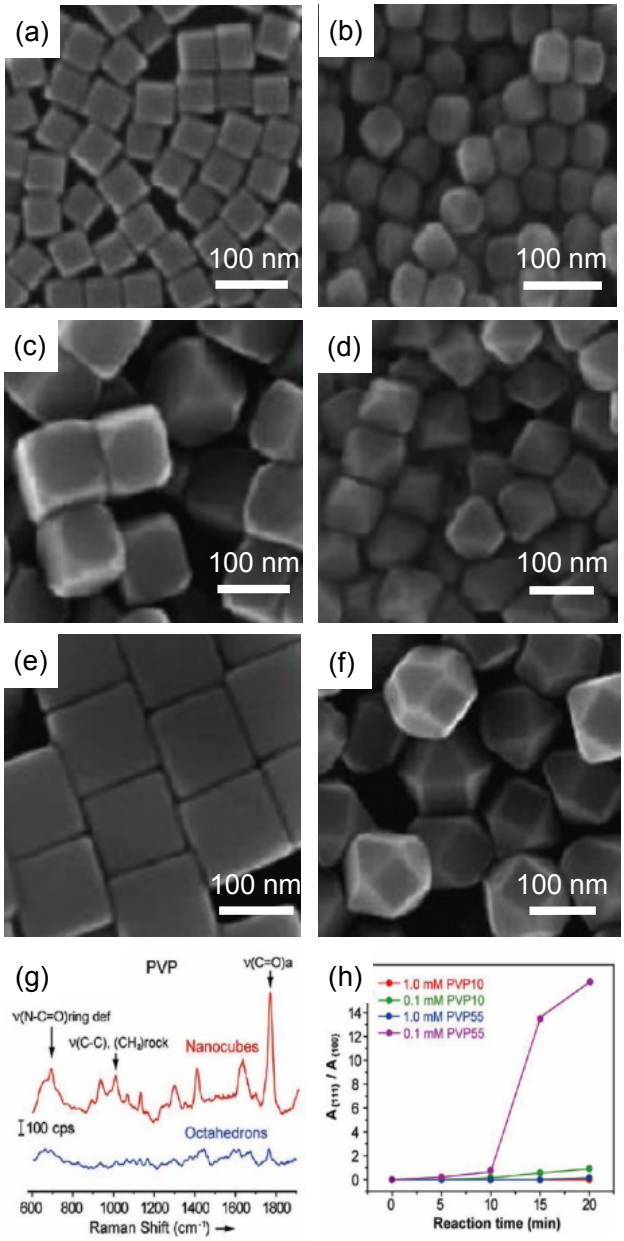

Fig. 3 SEM images of Ag nanostructures prepared with varying amounts PVP and different reaction times including (a) cubes (1.0 mM PVP55, 5 min), (b) truncated cubes (0.1 mM PVP55, 5 min), (c) truncated cubes (1.0 mM PVP55, 20 min), (d) octahedra (0.1 mM PVP55, 20 min), (e) cubes (1.0 mM PVP10, 20 min), (f) truncated octahedra (0.1 mM PVP10, 20 min). SERS spectra of (g) cubes and octahedra prepared in the presence of PVP55 and plot of (h) $A_{\{111\}}/A_{\{100\}}$ versus reaction time of Ag nanocrystals prepared at different concentrations of PVP10 and PVP55.[56] (reproduced with permission from ref. 56)

ranged from cubes to octahedra depending on the surface coverage density possible.[56] Many Ag NP syntheses have been conducted in EG, but solvent choice is also important. For

example, {100}-encased nanocrystals dominate when using EG, but {111}-encased nanocrystals are preferred with DMF.[56,66] The origin of this difference has been suggested to arise from the formidable reducing ability of DMF against metal ions.[69] 1-D, 2-D and 3-D Ag nanostructures can all readily be obtained using PVP-assisted methods.

PVP and gold nanoparticles. Au has also been intensely studied in NP form. The inclusion of colloidal Au as decorative elements to cups and bowls dates back nearly 2500 years.[32] In the mid-1800s, Michael Faraday described the synthesis of Au colloids.[70] In the twentieth century, two classic papers reported the synthesis of Au NPs. The first was the Turkevich method for producing Au spheres, which was published in 1951 soon after the advent of electron microscopy. Significantly, this work shows the prototype example that shape-controlled NPs could be achieved to a degree by varying the reducing agent.[71] The second was the work of Brust, who in 1994, demonstrated a two-phase method for synthesizing thiolate protected Au NPs.[72] $HAuCl_4$ was reduced with $NaBH_4$ in the presence of dodecanethiol, using tetraoctylammonium bromide as a phase-transfer agent. This resulted in Au nanospheres with diameters ranging from 1-3 nm.[72]

In the past two decades, reports on the synthesis and application of Au NPs have been abundant. This emphasis is driven by the fields of LSPR sensing, nanomedicine, and nanocatalysis.[32,33,73,74,75] One of the first reports of Au nanocrystals from a PVP-assisted process was by Yang and co-workers (Fig. 5a).[31] The Au nanocrystals were synthesized by injecting an EG solution of $HAuCl_4$ and an EG solution of PVP simultaneously into boiling EG. PVP was used as a shape-directing polymer and the resulting nanocrystals included triangular plates, truncated tetrahedra, icosahedra and octahedra. All structures displayed primarily {111} facets. The authors suggested that PVP preferentially adsorbed to Au(111) planes which reduced the growth rate along <111> directions and enhanced the growth rate along the <100> directions. Interestingly, when Ag^+ was introduced, cubes resulted which suggested that the growth rates along the <100> and <111> directions were reversed. These results show that PVP interacts differently with Au, stabilizing {111} facets, compared to the {100} facets of Ag.[31,56] A recent computational study using DFT an MD simulations of PVP monomer analogs adsorbing onto Au nanocrystals supports that PVP adsorption on Au(111) surfaces is thermodynamically favourable compared to PVP on Au(100).[76] DFT studies suggested that the pyrrolidone units bind to Au surfaces through the oxygen atom and that the binding energy is dominated by vdW interactions. The authors also noted that Au(100) reconstructs while Ag(100) does not, which could help explain why {111} facets are preferred in PVP-assisted Au nanocrystal syntheses, while {100} facets are preferred in PVP-assisted Ag nanocrystal syntheses.[76]

Micron-sized particles built from nanosized components have also been synthesized using PVP-assisted methods. Polycrystalline Au spheres composed of smaller NPs with an approximate diameter of 10 nm were achieved (Fig. 5b). PVP was used as a size-controlling agent, *o*-diaminobenzene as the reducing agent, and $HAuCl_4$ as the Au source under aqueous conditions at room temperature.[77] The spheres have narrow size distributions and the molar ratio of PVP to $HAuCl_4$ influenced the final size of the spheres. High ratios lead to smaller spheres, while low ratios lead to larger spheres.[77] A complete lack of PVP led to irregular-shaped aggregates. The authors proposed that high PVP concentrations could induce aggregation of the smaller NPs.[77]

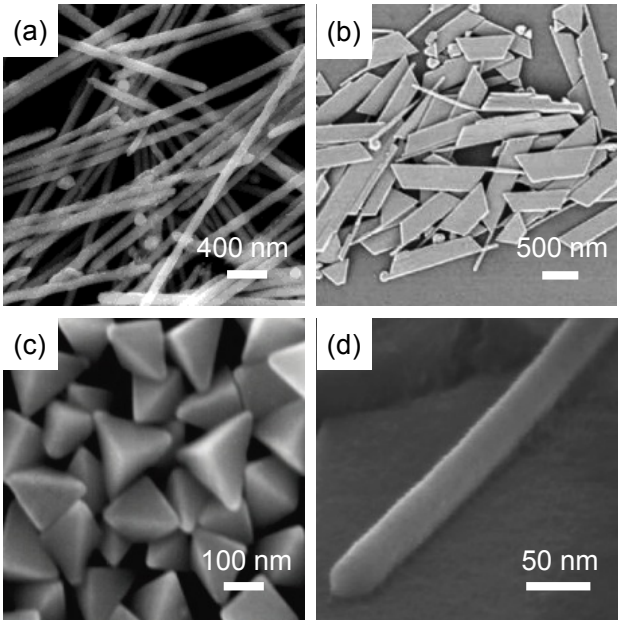

Fig. 4 SEM images of Ag nanocrystals prepared using PVP-assisted polyol and/or DMF syntheses showing morphologies of (a) wires,[60] (b) flags,[66] (c) bipyramids,[67] and (d) nanobeams.[68] (Figures (a), (b), (c) and (d) were reproduced with permission from ref. 60, 66, 67 and 68 respectively)

PVP-moderated syntheses in DMF have also yielded shape-controlled Au nanocrystals. Au octahedra (Fig. 5c) could be grown from Au nanorod seeds using PVP40, DMF, and $HAuCl_4$ as shown by Pastoriza-Santos, Liz-Marzán and co-workers.[78,79] Cetyltrimethylammonium bromide (CTAB) was used to synthesize the Au nanorods but replaced by PVP to prevent aggregation when the rods were transferred to DMF. A key step to the synthesis of the octahedra was reducing Au^{3+} to Au^+ prior to the introduction of the seeds in order to avoid oxidation of the Au seeds.[78,79] From TEM, SEM, selected area electron diffraction (SAED), and atomic force microscopy (AFM), the authors proposed that growth occurs in the order {100} > {110} > {111}.[78] The adsorption of PVP onto Au was suggested to alter the surface free energy of different facets and as such serves in a shape-directing role, where the product displayed only {111} facets. The structural change to octahedra from rods was suggested to occur as a way to minimize total surface energy.[79]

{111}-bound penta-twinned Au decahedra are also possible with PVP as a capping agent (Fig. 5d).[80] Xie, Lin, and co-workers showed that 180 nm Au decahedra are obtained by reducing $HAuCl_4$ in DMF with PVP40.[80] The reaction took place at 140 °C. The authors noted that there was no direct-evidence for PVP adsorbing to specific facets but suggested that with their synthesis in DMF with PVP40, the {111} facets of Au nanocrystals were most stable.[80]

The combined stabilizing and reducing properties of PVP also contribute to the synthesis of Au nanostructures. Au nanostars are fascinating structures due to the ability to tune their LSPRs by the number and aspect ratio of branches. The optical properties of Au nanostars arise from the hybridization of plasmons localized at the tips and cores.[81] Liz-Marzán and co-workers showed that Au nanostars could be obtained in

excellent yield with a PVP-moderated method.[82] Concentrated solutions of PVP in DMF were mixed with $HAuCl_4$ (the molar ratio of the repeating unit of PVP to Au atoms was ≥ 800) and PVP-coated Au seeds.[82] The reactions were at room temperature and the authors noted a final colour of blue.[82] A detailed study by Liz-Marzán and co-workers showed that the size of the Au nanostars (45-100 nm) could be readily tuned by changing the seed size (2-30 nm) and temperature (Fig. 5e).[81] Such synthetic control is significant as the sharpness and number of tips can influence the LSPR shape and position. The authors proposed that PVP reduced $HAuCl_4$ to deposit Au onto the seeds through a kinetically controlled process. PVP was also suggested to be responsible for shape-control by adsorbing and desorbing from the different crystal facets in a preferential sequence.[81,82] Though the molar ratio of precursor to seeds, R, did not affect whether branched structures grew, the number of tips on the nanostars increased with R (Fig. 5f).[81] The authors observed a blue-shift of the tip LSPR mode and decrease in intensity with decreasing R and an increase in core LSPR mode. The electric field enhancement of the tip LSPR mode is influenced by the size of the seeds, which in the case of Fig. 5f, was 30 nm.[81]

Many shape-controlled Au nanostructures are accessible through PVP-mediated syntheses. The PVP-Au interaction is stabilized by donation of a lone pair of electrons from the ntrogen or carbonyl oxygen of the PVP repeating unit into hybrid orbitals of the gold ions.[79] Yang and co-workers demonstrated one of the first large scale syntheses of Au nanocrystals using a PVP-assisted method that resulted in Au octahedra.[31] Liz-Marzán and colleagues showed that Au nanostars could be synthesized by using a system with a high molar ratio of PVP/$HAuCl_4$. They also noted that the molecular weight of PVP did not have a large effect on the formation of the Au nanostars.[82] Collectively, these results indicate that PVP preferentially adsorbs to {111} facets of Au nanocrystals in the absence of salts/foreign ions, which is different from the solvent-dependent preferential adsorption known for Ag nanocrystals.[31,56]

Platinum group and rhenium nanostructures prepared using PVP. Platinum group metals as NPs are useful industrial catalysts. For example, Pt-based catalysts have been used in nitric acid production for over a 100 years. A Pt/Rh (90/10) catalyst facilitates oxidation of ammonia, the first step in making nitric acid.[83] Pd and Pt are also in automobile catalytic converters, which convert CO and NOx into CO_2, N_2, and O_2. Proton exchange membrane (PEM) fuel cells such as direct methanol fuel cells (DMFC) and direct formic acid fuel cells (DFAFC) show promise as clean energy platforms. Pd and Pt provide high electrocatalytic activity of various fuels for PEM devices.[84,85] In comparing the two, Pd nanocatalysts are more resistant to poisoning by CO compared to Pt.[86] Also, hollow Pd nanospheres have been used in Suzuki coupling reactions as a reusable heterogenous catalyst.[87] Finally, supported Pt NPs have been used to catalyze hydrogenation of azo bonds.[88]

A seminal paper on shape-controlled Pt NPs by El-Sayed and co-workers in 1996 detailed findings of 5 shapes, including cubes, tetrahedra, icosahedra, irregular-prismatic, and cubo-octahedra.[89] Soon after, PVP-assisted syntheses of shape-controlled Pd and Pt nanostructures were reported from El-Sayed and co-workers,[90] Xia and co-workers,[91,92] and Yang and co-workers.[93] PVP binds to Pt surfaces through the carbonyl group or nitrogen atom of the repeating unit based off of UV-Raman and FTIR spectroscopy.[94] These works lay the foundation for studies into the shape-dependent catalytic properties of Pd and Pt nanocrystals, as outlined herein.

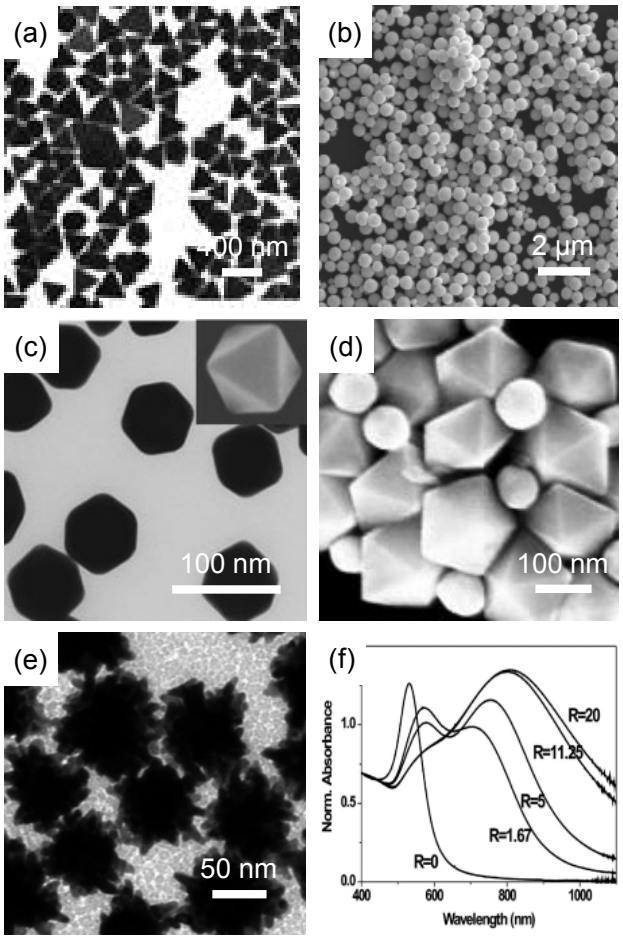

Fig. 5 SEM/TEM images of PVP-moderated shape-controlled gold nanostructures including (a) triangular plates,[31] (b) spheres,[77] (c) octahedra,[79] (d) decahedra,[80] (e) stars[81] and Vis-NIR spectra (f) of gold nanostars prepared using different ratios of seeds to salt concentration.[81] (Figures (a), (b), (c), (d) and (e-f) were reprinted with permission from ref. 31, 77, 79, 80 and 81 correspondingly)

Huang and Zheng developed a synthesis to Pd NWs and nanorods with a 5-fold twinned structure from the hydrothermal reaction of $PdCl_2$, NaI and PVP30.[95] Based off of HRTEM and ED, the authors suggested that the NWs were bound by 5 {100} facets and growth was along the [110] direction. The Pd NWs had an average diameter of 9.0 nm and were microns in length (Fig. 6a).[95] PVP had a dual role in the synthesis of the NWs. The first was as a reducing agent via the hydroxyl groups at the ends of the molecules. The second role of PVP was as a surface protecting agent which prevented the NWs from agglomerating together.[95] PVP concentration was also found to be vital as increasing or decreasing its concentration altered the resulting morphology from wires to spheres and rods or a mixture of triangles, bars, tetrahedra, and cubes.[95] These changes may arise from changes in the number of hydroxyl groups available as a reducing agent, altering the growth kinetics.[96]

Pd cubes, cuboctahedra and octahedra are also synthetically accessible using PVP-assisted methods and present an excellent opportunity for studying the effect of plane, edge, and corner atoms on catalyzed reactions. Uniform Pd nanocrystals of cubes, cuboctahedra and octahedra are also synthetically

accessible using PVP-assisted methods. Kiwi-Minsker and co-workers studied the hydrogenation of 2-methyl-3-butyn-2-ol (MBY) to 2-methyl-3-buten-2-ol (MBE) using Pd nanocrystals (Fig. 6b) synthesized by the reaction of Na_2PdCl_4, L-aa, KBr, and PVP.[97] The main function of PVP is as a stabilizing agent as PVP is too large to be effective as a shape-directing agent for the small Pd nanocrystals produced. Cuboctahedra usually result from PVP being used as a stabilizing agent for Pd NPs < 10 nm.[97] The bromine ions are more effective as capping agents on account of their small size, preferentially adsorbing to the {100} facets of Pd.[97] When larger Pd nanocubes are grown, ~ 48 nm edge length, PVP is effective at stabilizing the {100} facets and functions similar to what is observed in the PVP-Ag system.[1,92] The authors observed that the selectivity and activity of the catalyst was influenced by the coordination number of the atoms which differs on edge and plane sites. Simulations suggested that a cubic structure, 3-5 nm in size, is the ideal catalyst for semi-hydrogenation of MBY to MBE.

Metal nanoplates are anisotropic 2-D crystals with fascinating LSPR sensing properties. Xia and co-workers synthesized triangular and hexagonal Pd plates from the reduction of Na_2PdCl_4 by PVP in an aqueous solution heated for 3 hours at 100 °C. Sizes of the Pd nanoplates ranged from 50-80 nm (Fig. 6c).[98] They found the reducing ability of PVP is proportional to the number of hydroxyl end groups and hence the number of PVP molecules in solution.[98] When PVP is used as a reducing agent, the function has been suggested to be similar to that of a long chain alcohol.[98] The weak reducing ability of PVP leads to slow reduction of the Pd precursor, introducing stacking faults through kinetically controlled growth and resulting in {111}-bound nanoplates.[98] Similar 2-D nanoplates were produced when PVP was used as a reducing agent in a Ag system as well.[96]

Single-crystalline Pd arrow-headed tripods have also been synthesized using PVP-assisted synthesis.[99] Chen, He, and co-workers prepared the arrow-headed tripods under N_2 using PVP55, $Pd(acac)_2$, benzyl alcohol, and benzaldehyde at a reaction temperature of 70 °C (Fig. 6d).[99] PVP was in high concentration and functioned as a surfactant. The authors suggested that large amount of PVP in solution prevented small Pd grains from growing quickly. PVP passivated the entire surface of the Pd nanostructures through interaction of the carbonyl group and nitrogen atoms of the repeating unit.[94] This passivation maintains the structure which displays primarily {111} facets. The PVP can be removed from the surface of the Pd nanostructures by electrochemical cleaning, which is necessary for their use as electrocatalysts.[99]

Many shape-controlled Pt nanocrystals are also synthetically accessible by PVP-moderated methods.[90,91,93,94] For example, single-crystalline Pt nanoflowers were demonstrated by Wang, Zhang and co-workers.[100] The authors conducted a detailed study on the polyol synthesis (Fig. 6e) with H_2PtCl_6, KI, EG, and PVP58 at a temperature of 160 °C. PVP prevented agglomeration as its absence led to only large structures that were not stable in solution.[100] The Pt nanoflowers where ~25 nm in size and composed of smaller crystallites with {111} and {002} facets expressed as determined by SAED.[100]

Pt cubes and tetrahedra have also been synthesized using a PVP-assisted polyol process, as detailed by Yang, Somorjai and co-workers.[93,101] The synthesis was achieved by alternating injections of solutions of PVP55 in EG and H_2PtCl_6 into refluxing EG with $AgNO_3$.[93,101] Pt nanocubes were produced in ~ 80% yield (Fig. 6f) and they had a vertex-to-vertex distance of about 9 nm.[101] PVP55 served as a capping agent to control the growth of the Pt nanostructures. The PVP-Pt interaction occurs through the carbonyl group of the repeating unit. Somorjai, Rioux, and co-workers studied the PVP-Pt interaction on {100} facets using sum-frequency generation (SFG) vibrational spectroscopy.[101] The results suggested that the vinyl group is close to the Pt surface while the pyrrolidone group is tilted away; this configuration is similar to what is suggested for the PVP-Ag nanowire interaction.[22,101]

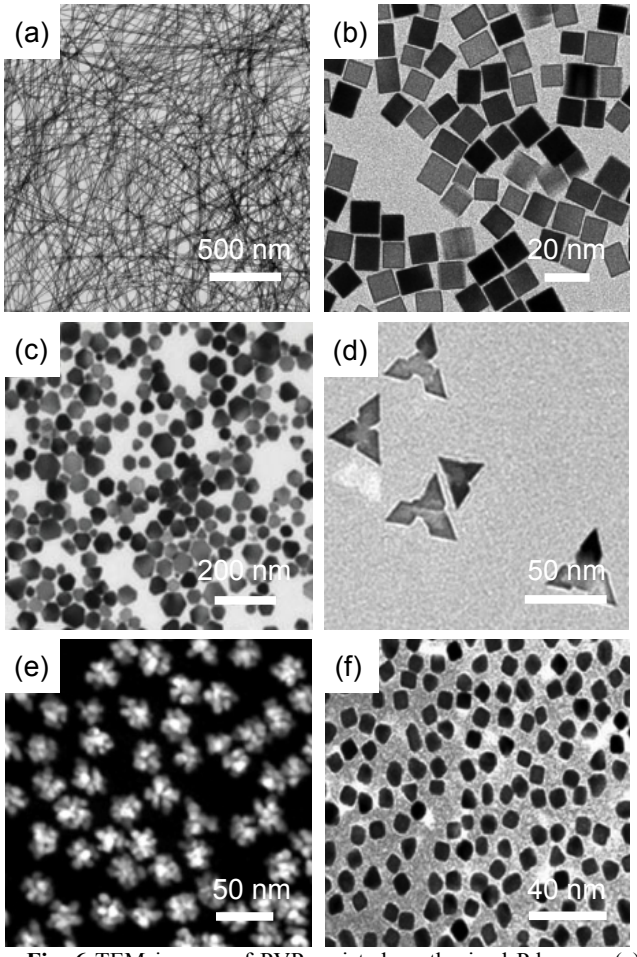

Fig. 6 TEM images of PVP-assisted synthesized Pd nano- (a) wires,[95] (b) cubes,[97] (c) plates[98] and (d) arrow-headed tripods[99] and TEM images of PVP-assisted synthesized Pt nano (e) flowers[100] and (f) cubes and tetrahedra.[101] (Figures (a), (b), (c), (d), (e) and (f) were reproduced with permission from ref. 95, 97, 98, 99, 100 and 101 respectively)

Finally, ruthenium (Ru) and rhenium (Re) NPs have been prepared in the presence of PVP. In particular, Novio *et al.* synthesized small Ru NPs (around 2 nm in size) stabilized with either PVP or dppb (bis(diphenylphosphinobutane) ligand. They investigated the coordination of carbon monoxide (CO) gas with the NPs surface through IR and solid-state NMR measurements, by applying an atmosphere of 0.5 bar of ^{13}CO at the NPs. It was found that CO groups are mobile on the surface of PVP-capped Ru, even in the solid state, but notably less mobile on dppb-capped Ru NPs, attributed to the bulky ancillary nature of the latter ligands which might make the fluxionality of CO more sluggish.[102] Philippot and co-workers published the synthesis of ultra-small (*ca*. 1-1.2 nm) Re NPs by H_2-mediated reduction of $[Re_2(C_3H_5)_4]$ at 120 °C in

the presence of either hexadecylamine (HDA) or PVP. The morphologies of the particles were similar, except HDA favored the formation of slightly elongated shapes in some cases. This preference was attributed to a soft template effect.[103]

PVP-assisted synthetic methods can lead to a variety of shape-controlled nanostructures for the platinum group metals.[90,91,93,94] Catalytically active metal nanocrystals with specifically exposed facets are sought after materials.[90,98] For example, in the synthesis of Pd and Pt nanostructures, PVP functions mainly as stabilizing agent to prevent agglomeration of the particles. PVP has limited ability as a shape-directing agent in the synthesis of nanostructures < 10 nm on account of its large size. Halide ions are more effective as small shape-directing agents.[98] When the Pd nanostructures become > 25 nm in edge length, PVP functions as a structure-directing agent in a manner similar to what is seen in the PVP-Ag system.[1] An interesting observation from Xia and co-workers is that PVP can also function as a reducing agent, facilitating Pd nanoplate formation in a manner similar to that observed for Ag nanoplates.[96,98]

Bimetallic nanostructures. Metals can be combined to enhance properties, such as making materials lighter, stronger, or more corrosion resistant. A widely used alloy is stainless steel, which consists of Cr and steel. A major advantage of stainless steel is high resistant to rusting. Solder, an alloy once primarily composed of Pb and Sn, is used to join metal junctions. Ni can be alloyed with many metals, including Fe and Mo to produce Mu-metal which shields against magnetic interferences. Enhancements in catalytic performance of metal nanostructures is possible by combining two metals through alloying or core@shell structures.[44,104] These structures can increase the number of active surface sites and alter the electronic structure of the material compared to the parent components.

Common bimetallic nanostructures include Au-Ag and Pd-Pt. Au and Ag are important plasmonic elements, have the same crystal structure, and nearly identical lattice constants of 0.408 nm and 0.409 nm, respectively.[105] Pt and Pd core@shell systems have produced active catalysts, which can be attributed to the bimetallic architecture.[104] Like the Au-Ag system, Pt and Pd have similar lattice constants of 0.392 nm and 0.389 nm, respectively, which minimizes strain. Pt-based alloys are the most common catalysts in PEM fuel cells due to their high activity towards the oxygen reduction reaction (ORR) and cost-effectiveness.[104,106] Both core@shell and alloyed nanostructures can be achieved with PVP-assisted methods.

Shape-controlled Au@Ag nanocrystals such as hexagonal plates (Fig. 7a) with primarily {111} facets were synthesized using a PVP-moderated two-step process.[105] In the first step, Au seeds were prepared by reduction of $HAuCl_4$ in EG, with concentrated PVP40 as a capping agent. Microwave (MW) heating produced nanocrystals in 3 minutes. The Au seeds included MTPs, octahedra, and plates.[105] Given the predominance of {111}-encased structures, the authors suggested that in an EG solution with MW heating, PVP selectively adsorbs onto {111} facets of Au similar to what was observed by Yang and co-workers for Au nanocrystals synthesized in boiling EG.[31] The Au seeds were combined with $AgNO_3$, DMF, and PVP1300 at a temperature of 140 °C. An epitaxial Ag shell was deposited. Here, PVP functioned as a shape-directing agent by binding preferentially to the {111} facets of the Ag shell. Interestingly, the primarily {111} bound Au seeds could be surrounded by a {100} faceted Ag shell by switching from DMF to EG in the second step,[105] A similar solvent effect was noted in the synthesis of Ag nanoflags.[66]

Another PVP-assisted core@shell system recently reported was of Au-Ag nanorings surrounded by triangular Ag shells (Fig. 7b).[107] The first step involved the synthesis of Ag triangular plates from the reduction of $AgNO_3$ in the presence of trisodium citrate (TSC), hydrogen peroxide, PVP58, and $NaBH_4$. PVP acted strictly to prevent agglomeration of the resulting nanoplates.[107] The Ag nanoplates were then transformed into Ag nanodisks by etching with NaCl then polycrystalline Au-Ag rings by galvanic replacement. The final step formed a Ag shell around the Au. TSC, PVP58, and $AgNO_3$ were added to an aqueous Au nanoring seed solution, followed by L-aa. TSC binds preferentially to the {111} facets of Ag on account of symmetry matching revealed by DFT calculations.[58,108] This interaction restricts vertical growth along the <100> directions of the nanostructures. PVP, in contrast, binds preferentially to the {100} facets of Ag,[56,58] which restricted the thickness of the plates to approximately 20 nm. When TSC was removed from the final step, Au nanorings encased with by Ag nanocubic shells were produced due to the preferential binding of PVP to {100} facets of Ag.[107] This example illustrates that PVP and TSC can be used cooperatively in a synthesis to fine tune structural features.

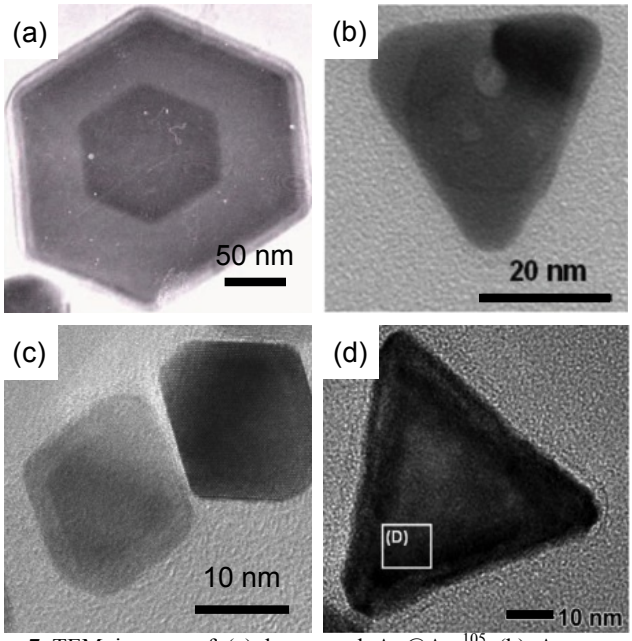

Fig. 7 TEM images of (a) hexagonal Au@Ag,[105] (b) Au nanoring@Ag,[107] (c) polyhedral Pt@Pd[110] and (d) Pd@Pt triangular plates.[111] (Figures (a), (b), (c) and (d) were reprinted with permission from ref. 105, 107, 110 and 111 respectively)

Very recently we reported the synthesis of bimetallic nanostructures composed of a plasmonic (Au) and a catalytic non-plasmonic (Pt) metal in the presence of PVP, using Pt nanodendrites as seeds. Core-satellite Pt@Au nanostructures were synthesized with PVP as a capping agent, while using CTAB yielded Pt-Au nanodimers. We attributed the core@satellite architecture to PVP facilitating nucleation on multiple seed features. In contrast, CTAB forms a complex with $AuCl_4^-$ ions, thus limiting the growth of Au at a single point of the Pt surface to form Pt-Au dimers.[109]

The stabilizing ability of PVP is also used to synthesize Pt and Pd core@shell nanostructures. Long and co-workers used a PVP-assisted polyol process to obtain a series of polyhedral Pt@Pd nanocrystals including octahedra as seen in Fig. 7c.[110] Pt octahedral seeds were synthesized by alternating injections

of solutions of PVP55 in EG and H_2PtCl_6 into refluxing EG with $AgNO_3$.[110] PVP stabilizes the Pt octahedra from agglomeration, while silver ions function as a shape-controlling agent by enhancing growth along the <100> directions of the Pt nanostructures.[93] The Pt seeds were then dispersed with Na_2PdCl_4 and PVP55 in EG to deposit the Pd shells. PVP again functioned as a stabilizing agent to prevent aggregation of the Pt@Pd nanostructures. The molar ratio of PVP to both metal precursors was kept constant at 12:1.[110]

As in monometallic nanocrystal syntheses, PVP can also serve dual roles as reductant and stabilizer in bimetallic syntheses. For example, Xia and co-workers synthesized Pd@Pt nanoplates by exploiting these features. First, Pd nanoplates were produced by slowly reducing Na_2PdCl_4 with PVP55 in aqueous conditions.[111] The weak reducing ability of PVP enables the kinetically controlled growth conditions necessary for nanoplate formation.[98] Next, Pt shells were deposited epitaxially by reducing H_2PtCl_6 with CA under aqueous conditions in the presence of PVP.[111] Nanoplate sizes ranged from 50-100 nm, with an average thickness of 24 nm. PVP was used as a stabilizing agent to prevent agglomeration of the Pd@Pt nanoplate structures (Fig. 7d).[111]

PVP can also act as a stabilizing and reducing agent in the synthesis of bimetallic alloyed nanocrystals. Pd is often alloyed with Pt to enhance the catalytic performance of the material relative to either metal alone. Pd-Pt alloyed nanocages (Fig. 8a) were synthesized by Xia and co-workers from Pd nanocubes which served as sacrificial templates.[112] The Pd nanocubes were synthesized from an aqueous solution of Na_2PdCl_4, L-aa, KBr, KCl, and PVP55, where PVP mainly prevents agglomeration of the ~10 nm Pd nanocrystals.[98] Pd-Pt cages were produced by a galvanic displacement coupled with co-reduction in which a solution of K_2PtCl_4 was injected into a heated aqueous solution of CA, KBr, and PVP.[112] The resulting morphologies depended on the reducing agents and concentrations of Na_2PdCl_4 and bromide anions, which controlled the rate of galvanic displacement.[112] Interestingly, when CA was removed, PVP assumed roles as both stabilizing agent and reducing agent, with concave cubic Pd-Pt structures with hollow interiors produced on account of PVP being a weaker reducing agent than CA.[112]

Additional utility of PVP as a reducing agent was demonstrated by Xia and co-workers in the synthesis of Pd-Pt alloy nanocrystals.[113] Equimolar quantities of Na_2PdCl_4 and K_2PtCl_4 were reduced simultaneously by PVP55 under aqueous conditions at 80 °C. The weak reducing power of PVP, limited by the number of available hydroxyl end groups,[96] resulted in different-shaped alloyed Pd-Pt twinned structures, including truncated triangular plates with {111} facets (Fig. 8b).[113] The authors suggested the evolution of twinned structures involved coalescence of small particles from the initial stages of reaction induced by the weak reducing ability of PVP.[113] ICP-MS analysis showed the composition of these plates was $Pd_{80}Pt_{20}$. However, when the reaction was changed to polyol conditions with EG as the solvent and stronger reducing agent, truncated Pd-Pt octahedra resulted. The composition of the truncated octahedra were $Pd_{54}Pt_{46}$.[113]

Shape-controlled Pt-Ni alloy nanocrystals have been synthesized by He and Li using a PVP-assisted hydrothermal method.[114] Pt-Ni alloy octahedra for example (Fig. 8c) were synthesized by heating a solution of containing $Pt(acac)_2$, $Ni(acac)_2$, PVP8, benzylalcohol, and benzoic acid for 12 hours at 150 °C.[114] The PVP served as a capping agent in this synthesis, which also enabled the nanocrystals to be readily dispersed in polar solvents and used as catalysts in hydrogenation reactions without further cleaning.[114]

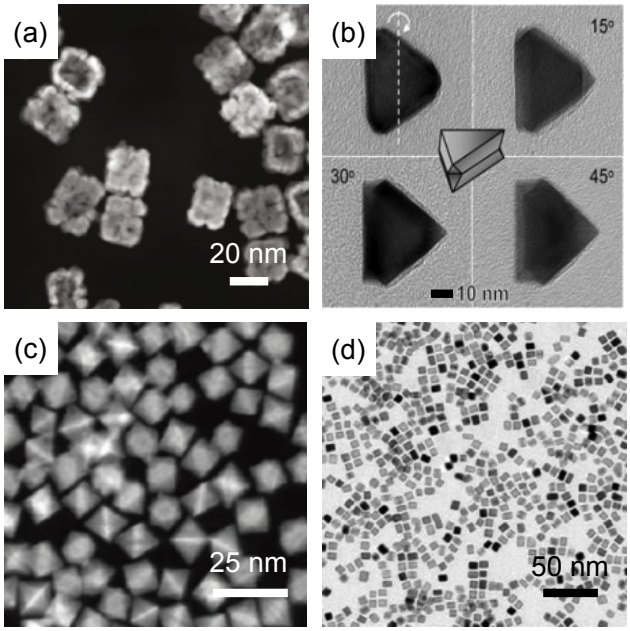

Fig. 8 TEM images of (a) Pd-Pt nanocages,[112] (b) Pd-Pt triangular nanoplates,[113] (c) Pt-Ni octahedrons[114] and (d) Pt-Pd cubes.[115] (Figures (a), (b), (c) and (d) were reprinted with permission from ref. 112, 113, 114 and 115 correspondingly)

PVP-assisted methods have also been used in the synthesis of highly-monodisperse Pt-Pd nanocrystals.[115] Huang and co-workers prepared the nanocubes by reducing equimolar amounts of Na_2PdCl_4 and K_2PtCl_4 in a solution of DMF, NaI, and PVP55 at a temperature of 130 °C.[115] ICP-AES and HRTEM measurements determined that the cubes (Fig. 8d) were $Pt_{51}Pd_{49}$ and had an average edge length of 7.2 nm. PVP protected the particles from agglomeration and the authors also suggested that PVP might enhance the shape-controlled synthesis along with main shape-directing agent, the halide ion.[115] When polyethylene glycol (PEG) or cetyltrimethylammonium chloride (CTAC) were substituted as the surfactant, agglomeration of the Pt-Pd nanocrystals resulted. The authors also noted that PVP alone could not reduce the precursors under the reaction conditions,[115] which contrasts with the work by Xia and co-workers where twinned Pd-Pt nanocrystals could be synthesized.[113] This difference suggests a dependence with solvent choice.

A variety of shape-controlled bimetallic structures can be synthesized, with PVP playing critical roles as stabilizing, capping, and reducing agents. In core@Ag systems, the choice of solvent influenced which facets of Ag were expressed, with {100} preferred in EG and {111} in DMF. These results are similar to observations from monometallic Ag nanocrystal synthesis.[56,58,105] Remarkably, the reducing capabilities of PVP in Pd-Pt systems were also found to depend on solvent choice.[113]

PVP for phase transfer and NP assembly. Assembly of metal nanostructures into ordered architectures is of interest due to the collective properties that can emerge and enhance applications in chemical sensing, catalysis, electronics, and metamaterials.[116,117,118,119,120,121] Langmuir-Blodgett-mediated assembly of metal NPs at the air/water interface has drawn

attention because of the large scale and long range ordered superlattices achieved (Fig. 9).[122,123,124] Such ordered monolayer assemblies can be transferred to solid substrate for further device applications (Fig. 9b).[122,123,124] Central to using this technique is the ability to disperse NPs in low polarity organic solvents, which can then spread onto a water surface. NP density can be manipulated by compression of the thin film. However, many metal NPs are prepared in water soluble media, requiring them to be transferred to the organic phase through chemical functionalization of the NPs.[124,125]

Interestingly, PVP-capped NPs are easily dispersed in organic medium such as chloroform, together with a small percentage of ethanol. Yang and co-workers[122,123] have explored the assembly of PVP-capped Ag NPs at the air/water interface using different building blocks (nanocubes, truncated cubes, octahedra, and NWs) (Fig. 9a-e). They demonstrated control of interparticle spacing, packing density, and superlattice symmetry; this structural control allows the optical response to be tuned over the entire visible range.[122] Such monolayer assemblies also exhibit excellent SERS activity, being used to detect arsenic from ground water.[126]

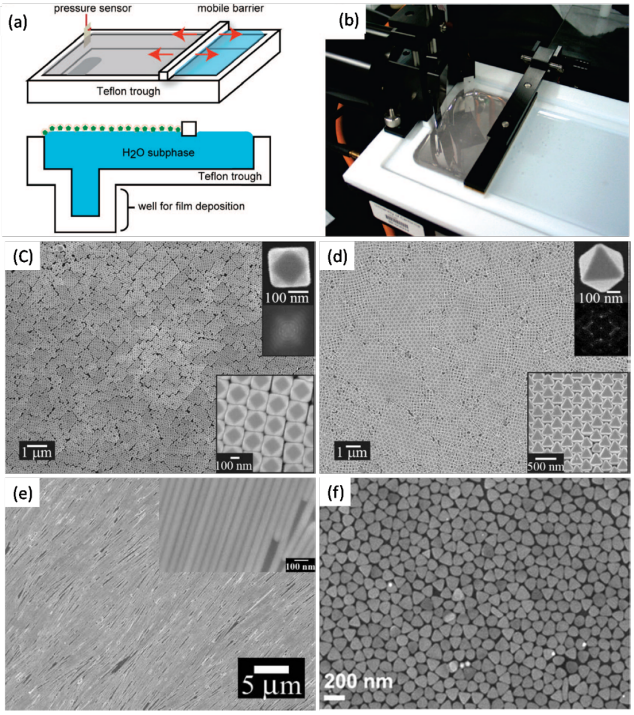

Fig. 9 (a) Schematic representation of water-filled Langmuir-Blodgett trough from the top and side views, (b) Image of the Langmuir-Blodgetttrough, in which the substrate is being pulled through Ag nanowire monolayer at the interface, (c-e) Superlattice made of different morphologies of NPs, prepared by the self-assembly at the air/water interface, (c) truncated Ag nanocubes, (d) Ag octahedra, (e) Ag NWs[122,123] and (f) self-assembled monolayer of Au nanoprisms prepared at the interface.[124] (reprinted and adapted with permission from ref. 122, 123 and 124)

The ease with which PVP-capped NPs can undergo phase transfer makes them ideal building blocks for many applications. For example, Ling and co-workers phase transferred Ag nanoprisms from water to an ethanol/chloroform mixture using PVP and then assembled the prisms into monolayer films for large-area, SERS-active substrates.[124] PVP-capped NPs can also be coated with silica shells using standard sol-gel chemistry in ethanol[127,14] (see also Fig. 14a). Many nanostructures have been coated with silica shells with this approach,[128] and Vanderkooy *et al.* reported an increase in silica shell thickness with increasing PVP molecular weight.[129] As these examples illustrate, PVP-capped NPs are dispersible in many solvents, opening possibilities in assembly and post-synthesis modification. Moreover, Lu *et al.* published an encapsulation process that allowed various kinds of nanoparticles (noble metals, metal oxides, metal chalcogenides) to be fully incorporated within crystals of a zeolitic imidazolate framework material (ZIF-8) in a well-dispersed manner. This approach included the functionalization of nanoparticle surfaces with PVP (Fig. 10) and the optimization of the crystallization of ZIF-8.[11]

Influence of PVP on catalytic and SERS active NPs. Capping molecules can interfere with the performance of NPs, particularly when molecules must adsorb or approach the metal surface for catalysis or chemical sensing. PVP can form a 1-2 nm shell at NP surfaces,[16] acting as a barrier to the NP surface from its environment. Thus, PVP often must be removed or replaced to enable specific applications.[130] Thiols can displace PVP, with the exchange process monitored by SERS spectra.[131] PVP-capped Ag and Au NPs have been extensively used for SERS-based sensing and detection. However, excess PVP on the NP surfaces can dampen the SERS enhancement. A thorough washing of PVP-capped metal NPs can allow strong SERS activity.[132] PVP can also influence the catalytic activity of NPs by blocking active sites. Thus, much effort has been dedicated to the removal of PVP from NP surfaces.[133,134,135] For example, Luo *et al.*[135] reported that PVP can be removed from Pt–Pd nanocubes by treating them with $NaBH_4$/tert-butylamine (TBA). The nanocubes retained their morphology, and their catalytic activity was improved. PVP can also be removed by H_2O_2/H_2SO_4 or heat treatment.[133,134] A recent review by Niu and Li discussed methods of PVP removal to improve nanocatalyst performance.[130]

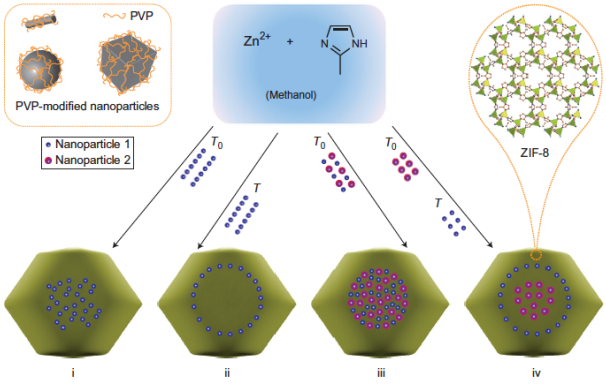

Fig. 10 Scheme of the controlled encapsulation of NPs in ZIF-8 crystals: Through surface modification with PVP, NPs with various morphologies and compositions are encapsulated in ZIF-8 crystals, themselves formed by assembling zinc ions with imidazolate ligands. The spatial distribution of incorporated PVP-modified NPs within ZIF-8 crystals can also be controlled by their addition sequence (that is, addition at the beginning of the MOF synthesis or during that process). Spatial distributions as a single type of NP in the central areas (i) or off the central areas (ii) of the MOF crystals, and as two types of NPs in the central areas (iii) or one type in the central area but the other type in the transition layers (iv) of the MOF crystals.[11] (reprinted with permission from ref. 11)

Influence of PVP on electrical properties. Finally, PVP-capped Ag NPs, especially Ag NWs, are used in flexible, transparent conductive electrodes for electronic applications (Fig. 11).[136,24,137] The Ag NW substrates are generally not conductive due to the capping PVP but can become so after annealing or application of mechanical pressing. For example, Tokuno *et al.*[136] demonstrated the transformation of non-conductive Ag NW substrates into conductive by the application of mechanical pressing after rinsing in water. The mechanical pressing leads to the decrease of sheet resistance through increased contact area of contact points between Ag NWs (Fig. 11b).[136] From the discussion, it is clear that the PVP could be effectively removed from the NPs surface after synthesis to apply them in various surface sensitive applications. Also, thorough washing of PVP-capped Ag NPs leads to conductive Ag films even at room temperature.[24] Clearly, PVP can be effectively removed from NP surfaces to enable the use of metal NPs in a variety of surface sensitive applications.

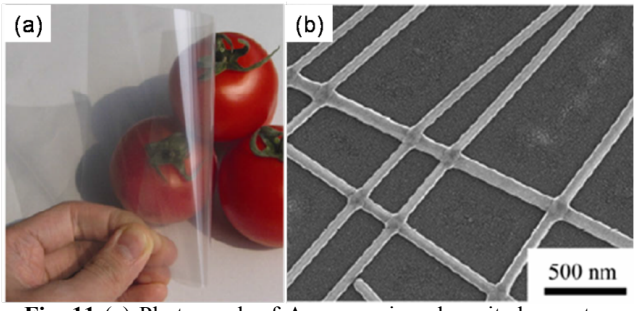

Fig. 11 (a) Photograph of Ag nanowires deposited on a transparent PET substrate and (b) FE-SEM images of Ag NWs on a PET substrate after mechanical processing.[136] (Reproduced with permission from ref. 136)

PVP and metal NP synthesis – A summary. PVP is a versatile reagent in the shape-controlled synthesis of monometallic and bimetallic nanocrystals. The PVP-metal interaction occurs through the carbonyl oxygen or nitrogen atoms of the repeating unit and the metal surface based off of XPS, Raman spectroscopy, FTIR spectroscopy and theoretical studies.[22,45,46,47,76,94] Many nanostructures are accessible, including cubes, cuboctahedra, octahedra, nanostars, wires, flowers, and twinned plates.[48,56,57,59,61,81,82,100,113] The first quantitative study of PVP in Ag nanocrystal growth was provided by Xia and co-workers. They found that the molecular weight and concentration of PVP dictate surface coverage, which in turn accounts for the formation of cubes, octahedra, and their intermediates.[56] Interestingly, the nature of the PVP-surface interaction depends on both the metal[31] and solvent being used. The former is accounted for by the degree of surface energy stabilization possible. The latter is less studied but may arise from the amphiphilic nature of PVP. Finally, the weak reducing ability of PVP, limited by the number of hydroxyl end groups, can be exploited to achieve kinetically controlled growth conditions.[96,98,113]

3. PVP in the synthesis of metal oxide NPs

Metal oxide nanoparticles is another category of nanomaterials which are prepared in the presence of PVP. These oxides include compounds as iron oxides, more complex ferrites, as well as other transition metal and main group metal oxides, but also rare-earth metal oxides. Also in this type of materials, PVP acts as stabilizer, preventing particle aggregation, but also it can kinetically control the growth of specific facets by binding onto others. Its concentration can also affect the particle morphology. In addition, PVP acts also here as dispersant and reducing agent under certain conditions, while its biocompatibility allows it to be used as capping agent for superparamagnetic iron oxide NPs targeted for magnetic resonance imaging (MRI) applications.[138]

Iron oxides and ferrites. Iron oxide nanoparticles such as magnetite (Fe_3O_4) and maghemite (γ-Fe_2O_3) draw a continuous interest owing to their properties such as biocompatibility, chemical stability and superparamagnetism which make them suitable for applications in domains as medical diagnosis and therapeutics, catalysis, sensors and magnetic storage devices. Single-crystalline Fe_3O_4 NPs with uniform size have been synthesized by a co-precipitation route using ferrous and ferric ions with PVP. The addition of PVP effectively decreased the coalescence between magnetite NPs, thus achieving uniform particle size.[139] Co-precipitation was also used to produce ultra-small Fe_3O_4 NPs from ferrous sulfate and iron sulfate, with sizes from 6.5 to 1.9 nm. The pyrrolidone functional groups of PVP could easily arrest crystals of Fe_3O_4 NPs, facilitating the formation of such small-sized NPs and hindering their aggregation. FTIR spectroscopy revealed excessive free PVP molecules in the samples after synthesis despite repeated washes; this excess polymer prevents aggregation.[140] A one-step solvothermal process to Fe_3O_4 nanoplatelets was published by Liu and Kim and employed PVP, ethylenediamine, and Fe(III)-urea complexes. The authors proposed that PVP influences the relative growth rates of different facets through polymer adsorption-desorption, contributing to morphology development.[141]

Fe_3O_4 NWs were prepared hydrothermally by Zhang *et al.* from $FeCl_2$ with PVP, diamine hydrate, and NaOH under a low magnetic field (0.035 T). The anisotropic shape was attributed to cooperation between a magnetic field-induced effect and PVP serving as a soft-template, as control experiments either without the magnetic field or without PVP, resulted in different particle shapes (square and hexagonal).[142] Gao and co-workers synthesized Fe_3O_4 nanocrystals by pyrolysis of $Fe(acac)_3$ in N-vinyl-2-pyrrolidone, which was polymerized in-situ to PVP. The Fe_3O_4 nanocrystals could be dispersed in many organic solvents and water on account of the PVP capping.[143] Moreover, PVP-coated iron oxide (phase denoted simply as 'spinel ferrite' by the authors) NPs synthesized by 'hot-injection' of $Fe(CO)_5$ in a PVP-DMF mixture were evaluated as promising materials for magnetic resonance imaging.[144]

Superparamagnetic Fe_3O_4 NPs between 8-11 nm were synthesized by a solvothermal approach in EG, using $Fe(acac)_3$ as the precursor, while PVP alone or combined with hexadecylamine or trioctylphosphine oxide were also incorporated. The magnetic properties of the various NPs were compared according to the monosurfactant or surfactant pair used.[145] The same iron source was also employed to acquire sub-5 nm Fe_3O_4 NPs with PVP and hexadecanediol in octylether solvent.[146] Diethyleneglycol (DEG) is also an effective solvent with PVP, with crystalline and water-soluble Fe_3O_4 NPs produced above 200 ^oC.[147]

Hematite, α-Fe_2O_3, NPs also have been synthesized with the use of PVP. $Fe(NO_3)_3$ was used as the iron source, with DMF as the solvent. The mixture was heated in an autoclave at 180 ^oC for 30 min. PVP stabilized and dispersed the α-Fe_2O_3 NPs,

and directed them toward quasi-cubic shapes (Fig. 12b).[148] These NPs could be built upon to achieve α-Fe_2O_3@SiO_2@Au nanocomposites which combined optical, superparamagnetic and catalytic activity.[149]

Ferrite nanostructures, *e.g.* $CoFe_2O_4$ NPs can also be synthesized using PVP as surfactant through a sol-gel procedure. Various concentrations of PVP were tested, and the resultant magnetic properties were studied. Coercivity (H_c) and saturation magnetization (M_s) showed a trend to increase with increasing PVP concentration.[150] The tertiary amide groups of the PVP molecules helped to disperse the NPs while the polar groups had strong affinity for iron and cobalt ions. The metallic ions are attracted by the polar group of PVP and distributed in the cavities of polymer chains (Fig. 13). This distribution favours solid solution formation. Sol-gel auto-combustion was used by Kurtan *et al.* to produce PVP-$CoFe_2O_4$ nanocomposites from $Co(NO_3)_2$, $Fe(NO_3)_3$, CA and EG. SEM analysis revealed the roughly spherical shape of the particles, whereas magnetic measurements with a vibrating sample magnetometer indicated the existence of cubic magnetocrystalline anisotropy according to the Stoner-Wohlfarth model.[151] Rivas and co-workers prepared PVP-$CoFe_2O_4$ nanocomposites under dilute PVP conditions (ferrite-to-PVP mass ratio < 0.1) by solvothermal decomposition of $Co(acac)_3$ and $Fe(acac)_3$.[152] These researchers noticed different magnetic behaviours among the $CoFe_2O_4$-PVP nanocomposites prepared using small or large $CoFe_2O_4$ NPs. Hollow $CoFe_2O_4$ spheres composed of smaller NPs were synthesized solvothermally with either PVP or PEG, together with oleic acid, NaAc, $FeCl_3$ and $CoCl_2$ at 200 ^oC.[153]

A solvothermal route was used also for the preparation of $Co_{0.8}Ni_{0.2}Fe_2O_4$ NPs with EG as solvent. The as-prepared NPs were modified by silane A and the resulting materials were dispersed ultrasonically in a PVP-ethanol solution to yield $Co_{0.8}Ni_{0.2}Fe_2O_4$/PVP composite nanofibers.[154] $ZnFe_2O_4$ and Fe_3O_4 nanospheres were produced in EG/DEG mixture, with PVP as a surfactant and metal chlorides as precursors. PVP was thought to strongly adsorb on the surface of the ferrite nanocrystals, limiting grain growth. Moreover, PVP use led to increased magneto-crystalline anisotropy in the samples.[155] PVP has been also used to prepare $NiFe_2O_4$ NPs by co-precipitation of iron- and nickel- nitrates, with hydrazine as a reducing agent and water as a solvent at 80 ^oC.[156]

Like $CoFe_2O_4$, sol-gel autocombustion can be used to prepare PVP-$MnFe_2O_4$ nanocomposites, in this case from PVP, $Mn(NO_3)_2$, $Fe(NO_3)_3$, CA, and EG. The final solution was stirred for 3 h at room temperature, and a gel was obtained after drying.[157] Other magnetic metal oxide nanostructures synthesized with PVP are NiO, CoO and Mn_3O_4. A distinct example includes Fe-doped NiO nanofibers (Fig. 12c) prepared by electrospinning $Ni(ac)_2$ and $Fe(NO_3)_3$ with $LiNO_3$, PVP, alcohol and water. The produced nanofibers exhibited room temperature ferromagnetism, but no metallic iron was evidenced. Therefore, such ferromagnetic behavior was considered inherent to the nanofibers.[158] PVP was also effectively used with oleic acid and oleylamine, common hydrophobic surfactants, to prepare quasi-spherical CoO nanocrystals by thermal decomposition of $Co(acac)_2$ in octadecene at 260 ^oC.[159] Finally, Toprak and co-workers reported the synthesis of PVP-Mn_3O_4 nanocomposites by heating a mixture of $Mn(acac)_3$, 1,2-hexadecanediol and PVP in diethyl ether at 120 ^oC for 2 h. The solution was then raised to 260 ^oC and the mixture was refluxed for another 2 h.[160]

Other transition and main group metal oxides. Another class of oxide materials prepared in the nanoscale using PVP are materials such as ZnO and TiO_2. These nanostructures exhibit remarkable optical properties and find applications in various fields, such as photocatalysis. An aqueous solution of $Zn(NO_3)_2$, methenamine, and PVP was heated in an autoclave at 95 ^oC for 6 h. ZnO nanorods (Fig. 12f) were produced, and the concentration of PVP was found to influence the length and diameters of the rods. In fact, increasing PVP, increases the viscosity of the reaction medium. The enhanced viscosity largely restricts the diffusion and growth process associated with the nanocrystal generation. Therefore the density of rods was decreased when PVP concentration was higher than 1 mM.[161] ZnO nanorods were also produced from $ZnSO_4$, sodium bicarbonate, water, and PVP via precipitation. The product could be modified with daunorubicin and the resulting material exhibited remarkable cytotoxicity and photodynamic effect for potential clinical and biomedical applications.[162] Precipitation methods were also used to prepare ZnO and Ni-doped ZnO nanorods from $Zn(ac)_2$, $Ni(NO_3)_3$, NaOH and PVP in aqueous solution. Hydrogenated samples possess high crystallinity and good optical properties for nano-optoelectronic devices like tunable light emitting diodes.[163] A simple hydrothermal route was used to synthesize nanocrystalline PVP-ZnO composite films from Zn foil. The product was comprised of 100 nm cube-like ZnO NPs embedded in a PVP matrix. PVP improved the crystal quality and reduced the amount of oxygen vacancies.[164] Furthermore, $Zn(ac)_2$, PVP, and NaOH was used to prepare ZnO NPs which were afterwards coated by SiO_2. PVP was suggested to play a critical role as a versatile coupling agent for a fast and simple way to develop the silica shells. More specifically, it was suggested that the formation of C-O^- groups in PVP molecules played an important role for the growth of ZnO NPs and that the hydrogen bonding between the OH groups on hydrolyzed TEOS and C=O groups in PVP molecules was the key force for PVP to act as a coupling agent between ZnO and SiO_2 layers.[165] Wurtzite ZnO NPs were synthesized by a sol-gel method from $Zn(ac)_2$, methanol, and LiOH. Capping of the NPs with PVP was achieved during or after synthesis. The particles were then blended with poly(3-hexylthiophene), P3HT, for hybrid solar cells applications. Such blend was prepared by mixing P3HT and ZnO NPs solutions in chlorobenzene and the resulting solution was spin-coated onto glass substrates.[166] Selvam and Sundrarajan functionalized cotton with PVP-capped ZnO NPs. PVP played a dual role. First, the reactive dyeing capacity of the modified cotton fabrics was enhanced by using PVP as this compound is thermally fixed on the fabric in curing and PVP acts as an adhesive agent between dye and fiber. Second, the antibacterial activity of the whole material was also increased with the use of PVP as this polymer has been reported to inhibit the growth of bacteria in its medium.[51] Finally, ZnO/Ag nanocomposites can form by stirring ZnO colloids with PVP followed by the addition of a $AgNO_3$ solution. Heating at 60 ^oC for 12 h forms a gel. Apart from its surface-functionalization role, PVP assisted the reduction of $AgNO_3$ to Ag(0). The optical properties and the morphology of the formed nanocomposite also depended on the amount of PVP used. In particular, there was a slight blue shift of band-gap emission with the increase of PVP amount. Concerning morphology, a tendency for more elongated or dumbbell shapes with lower agglomeration was observed by increasing the PVP concentration up to 0.15 and 0.5 mM respectively.[167]

Titania (TiO_2) NPs and their surface functionalization with PVP have also drawn interest on account of their potential applications in cosmetics, photocatalysis and nanomedicine. Archana *et al.* presented a new dressing for wound care that consists of the biopolymer chitosan, PVP, and TiO_2 NPs. This composite exhibits antibacterial efficacy against four pathogenic bacteria while being non-toxic toward NIH3T3 and L929 fibroblast cells.[168] Chen and colleagues reported 2D nanosheets from nanomosaic building blocks of anatase TiO_2 nanosheets with exposed (001) facets. Titanium isopropoxide was used as precursor and HF served as a fluoride donor. PVP adsorbed on the {001} facets, hampering their growth. The size of the 2-D nanomosaics was controlled by reaction time, and the PVP concentration affected the nanostructure morphology as PVP acted like an efficient linker that brings adjacent nanosheets together for controlled lateral fusion. An increased amount of PVP would not only facilitate the lateral attachment of nanomosaics, but also coordinate the assembly of the large 2-D structures into more complex 3-D hierarchical architectures with flower-like shape.[169] The same titanium source was also used to prepare PVP-capped TiO_2 nanostrips with EG as solvent and water as a hydrolyzing agent. The nanomaterials had a blue shifted absorption edge and considerable photocatalytic activity toward Rhodamine B degradation.[170] A PVP-assisted sol-gel reaction was employed for the preparation of $Ag/AgBr/TiO_2$ nanocomposites at room temperature. $AgNO_3$, KBr and tetra-butyl titanate were the sources of silver, bromine, and titanium respectively. In this process, PVP was a dispersant, ensuring the creation of small particles, but also as a reducing agent for Ag^+ to Ag(0). The composite was very active toward photocatalytic degradation of Rhodamine B.[171]

Cu_2O nanostructures are of interest due to the inherent properties of this material. For instance, its small band gap allows applications in solar energy conversion, photocatalysis and gas-sensing, among others. Cu_2O spheres, rods and cubes were prepared by reduction of $Cu(NO_3)_2$ with EG in the presence of PVP. PVP selectively adsorbed on the surfaces of Cu_2O, providing a means of morphology control. The authors speculated that PVP adsorption onto specific faces of Cu_2O altered their growth rates, thus enabling also the generation of non-spherical shapes.[172] $CuSO_4$ and NaOH were used as reagents in the hydrothermal synthesis of PVP-capped Cu_2O nanoflowers. The authors attributed this morphology to templating, guided by PVP, which assembled 'petals' into rose-like structures.[173] Gram-scale synthesis of Cu_2O nanocubes by hot-injection of a $Cu(acac)_2$ solution into a PVP-pentanediol solution at 240 ^oC was reported by Song and colleagues. The Cu_2O could be oxidized to CuO by treatment with ammonia solution, ethanol and NaOH to produce hollow and branched nanostructures. The final nanoparticles were employed as Li-ion battery anode materials.[174] EG and PVP were used to synthesize Cu_2O nanospheres and nanocubes by reduction of $Cu(NO_3)_2$. The latter shape was only obtained upon addition of NaCl before $Cu(NO_3)_2$ in the reaction solution. PVP served as colloidal stabilizer whereas EG acted as dispersing medium and reductant.[175] In a somewhat different approach, a Cu plate was submerged in an aqueous solution of PVP surfactant. Cu_2O NPs were generated by laser ablation of the plate with the first harmonic of a Nd:YAG pulsed laser.[176]

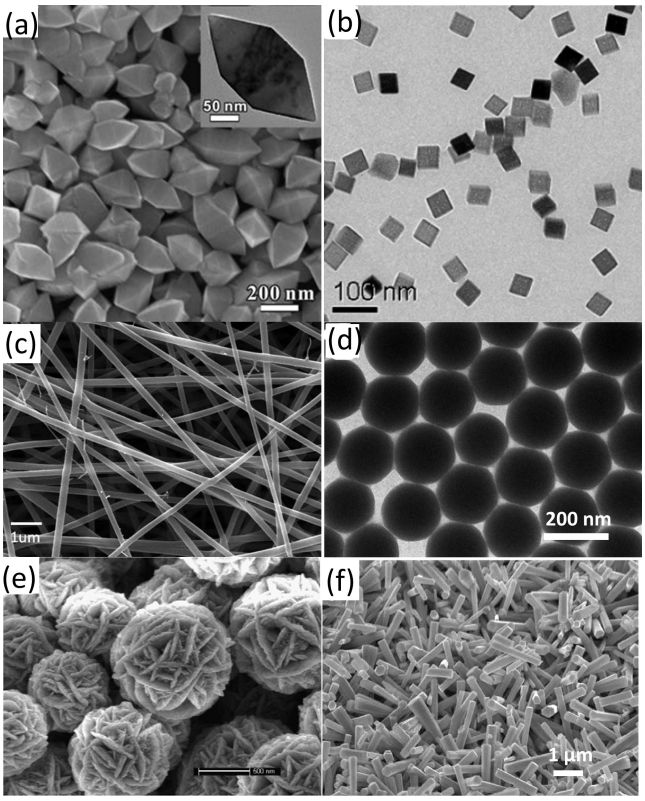

Fig. 12 (a) SEM image of SnO_2 NPs synthesized by hydrolysis of $SnCl_4$,[177] (b) TEM image of quasicubic α-Fe_2O_3 NPs,[148] (c) SEM image of Fe- and Li- co-doped NiO/PVP composite nanofibers before calcination,[158] (d) TEM image of Y_2O_3 sub-micron spheres,[183] (e) SEM image of CdS walnut-like structures,[184] and (f) TEM image of ZnO rods.[161] (Figures (a), (b), (c), (d), (e) and (f) were reproduced with permission from ref. 177, 148, 158, 183, 184 and 161 respectively)

Several other oxides have been synthesized using PVP. For example Han *et al.* reported a simple method for the preparation of octahedral SnO_2 particles (Fig. 12a) with high-index {221} facets through a hydrothermal route at 200 ^oC for 12 h, with $SnCl_4$ as tin source. In that reaction PVP had a significant role in dispersing the SnO_2 particles, rather than in morphology control.[177] Monodisperse rutile GeO_2 NPs can also be obtained via a facile hydrothermal process using PVP; The PVP helped to direct particle shape and its use provided enhanced luminescence properties compared to NPs not capped by PVP. This result was assigned to PVP surface passivation that minimized surface defects and increased the possibility of electron-hole recombination.[178]

Rare-earth oxides. Rare-earth oxide NPs have attracted attention due to their excellent catalytic properties and their possible applications in biological fields. Ceria (CeO_2) is useful in catalysis, electrochemistry and optics. Also, ceria-based materials absorb strongly in the UV and can be used to protect human skin from sun exposure. Si *et al.* reported an alcohothermal synthesis of 4 nm CeO_2 colloids using PVP as a stabilizer, an alkylamine (triethylamine, butylamine or hexadecylamine) as base and $Ce(NO_3)_3$ as the precursor.[15] Hollow CeO_2 spheres were prepared from $CeCl_3$ employing also PVP and hydrogen peroxide. The influence of PVP on NP architecture was studied and found to influence the nucleation of the primary nanocrystals, although the authors indicated

that its exact role should be further investigated.[179] Itoh and colleagues fabricated hybrid films of pentaerythritol triacrylate (PETA) with PVP-capped CeO_2 NPs. These researchers suggested that the PVP shell facilitated enwrapping by the PETA matrix. The film showed excellent UV-blocking and visible light-transmission properties.[180] Cerium (III) acetate was employed by Phoka and co-workers for the preparation of CeO_2 NPs in the presence of PVP.[181] The same group reported monodisperse CeO_2 nanospheres by hydrothermal treatment of $Ce(NO_3)_3$ with PVP present. The NPs showed ferromagnetic properties at room temperature, with oxygen vacancies involved in the ferromagnetic exchange. The authors compared the behavior of several compounds used as cerium sources, and they found that the use of $Ce(NO_3)_3$ resulted in CeO_2 nanospheres with unifom size, probably thanks to a particular chelating mode of PVP with this precursor, leading to controlled nucleation and adsorption of PVP on various crystallographic planes of the growing crystals.[182]

Monodisperse lanthanide oxide sub-micron spheres were obtained through a hydrothermal route with PVP (Fig. 12d). Water-soluble Y_2O_3:Eu^{3+} uniform spheres could also be prepared via the same method by simultaneously using Y_2O_3 and Eu_2O_3 as starting materials. The role of PVP was critical for the particles morphology, since, upon its absence, only aggregated particles were observed.[183]

4. Metal chalcogenide nanostructures with PVP

PVP serves as an excellent stabilizer and shape-directing agent also during metal chalcogenide (MC) NPs synthesis preventing their aggregation and passivating surface states. In addition, PVP can chelate with small ions, suppressing NP growth and resulting in extremely small particle sizes. With their size-dependent optical properties, MC NPs are being studied for photoluminescence and photocatalytic applications, where the use of PVP can enhance their optical properties under certain conditions.

Metal sulfide NPs. The most common chalcogenide element combined with metals in the form of NPs is sulfur. Several metal sulfide NPs have been synthesized in the presence of PVP. For example, walnut-like CdS NPs (Fig. 12e) were produced by a solvothermal method with PVP as a stabilizer and $CdCl_2$ and sodium thiosulfate as precursors. The amount of PVP used was tuned aiming for optimum morphological, chemical and optical features.[184] Pattabi *et al.* prepared PVP-capped CdS NPs via a non-aqueous method with $Cd(NO_3)_2$ and H_2S precursors.[185] Polyvinyl alcohol (PVA), PVP and solvents methanol and DMF were employed for the preparation of PVP-CdS-PVA composites. The final material exhibited stronger and narrower band-edge emission rather than more typical defect-related emission. The latter emission could be quenched completely by optimizing the amount of PVP.[186] Saravanan and colleagues synthesized PVP-coated CdS NPs using cadmium acetate and sodium sulphide precursors. PVP modified the kinetics of Ostwald ripening such that the NP growth rate decreased with the size of the NPs, narrowing the size distribution. The enhanced luminescence properties of the PVP-capped CdS NPs in comparison to the uncapped CdS nanocrystallites were attributed to the PVP-coating; such coating lowered the amount of surface defects and increased the probability of electron-hole recombination.[187]

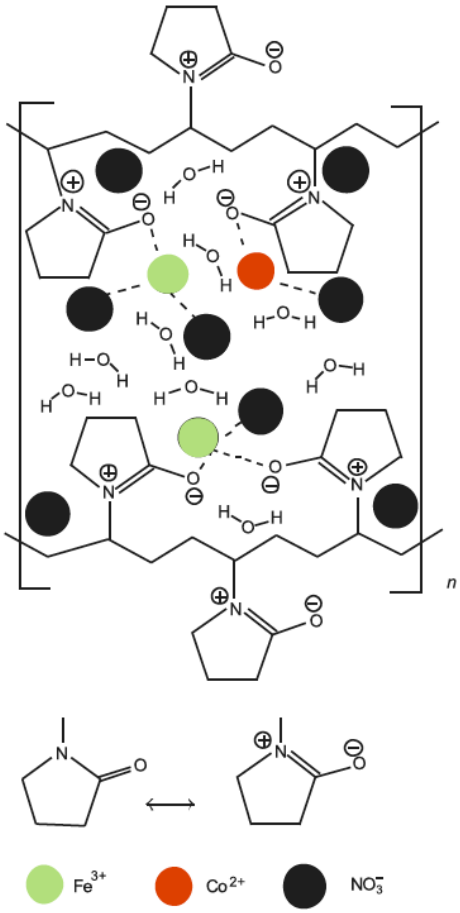

Fig. 13 Distribution of metallic ions and nitrate in the cavities of PVP – The case of $CoFe_2O_4$ NPs.[150] (reproduced with permission from ref. 150)

The shape of CdS NPs could be tuned to nanorods as demonstrated by Gaorong and colleagues with a PVP-assisted solvothermal synthesis with $CdCl_2$ and thiourea precursors. The quantity of PVP employed was crucial for the control of the shape and the optical behaviour of the NPs. In particular, a high concentration of PVP favoured the formation of elongated nanostructures, but an extremely high PVP concentration suppressed the particle growth in all directions. Concerning the optical properties, the surface emission was high if too much or too little PVP was used, due to unwanted capping or incomplete capping.[188] CdS/HgS/CdS nanocrystals were reported by Schill and El-Sayed through a three-step process: The CdS core was grown in methanol in the presence of PVP, afterwards the outermost cadmium atoms were exchanged for Hg to form a HgS monolayer. Finally, the binary NPs were capped with monolayers of CdS.[189] Soltani *et al.* synthesized CdS (and ZnS) NPs with cadmium chloride (or zinc acetate), PVP, and thioacetamide as sulfur source. These authors carried out a series of experiments by physically mixing different amounts of PVP-capped CdS and ZnS NPs so as to improve the photocatalytic activity of their product toward the degradation of methylene blue dye. PVP as capping agent contributed toward an improved photo-activity and photocatalytic performance.[190] Finally, Qin *et al.* prepared PVP-capped metal sulfide nanoboxes (CdS, Ag_2S, PbS, ZnS and $AgInS_2$) via two steps of ion exchange by a sacrificial template-directed method based on the Kirkendall effect and

Pearson hardness. The concentration of PVP influenced the particles morphology. For instance, without PVP irregular aggregated Ag_2S NPs were acquired.[191]

1-D copper sulfide microstructures were prepared by a microwave hydrothermal method in the presence of PVP. Thiourea and $Cu(NO_3)_2$ were used as precursors. The formation of rods was favored at high PVP concentrations. The C=O bonds within the PVP molecules were speculated to chelate with Cu^{2+}, hindering fast crystal growth and resulting in smaller crystallite sizes.[192] The influence of several anions and PVP on the transformation mechanisms of thiourea in EG solution was investigated by Fang *et al.* For this purpose, four copper precursors were employed: $Cu(NO_3)_2$, $CuCl_2$, CuCl and $CuBr_2$. Distinct phase tuning for the obtained NPs (*e.g.* hexagonal or cubic Cu-S crystal structure with varying Cu/S ratio) was observed as a function of precursor used.[193] CuS, SnS, and ZnS nanostructures were prepared by conventional hydrothermal and microwave hydrothermal methods employing thioacetamide as a sulfide source. Several control experiments were performed to study the effect of PVP on particle size. For instance, small ZnS NPs were obtained when PVP was employed to synthesize them, but without PVP the particle size was very large.[194]

Moreover, chalcopyrite ($CuFeS_2$) sheet-like and rod-like nanostructures were synthesized using $CuCl_2$, $FeSO_4$, $SC(NH_2)_2$ and PVP via a solvothermal process. It was found that an increased PVP quantity during synthesis improved the electrochemical activity of the $CuFeS_2$ NPs as Li-ion battery anode materials.[17] Cao *et al.* described the solvothermal synthesis of uniform Cu_2FeSnS_4 nanospheres in EG, with PVP as surfactant. Several reaction parameters were screened (*e.g.* amount of PVP or EG, reaction temperature, reaction duration) to achieve particles with homogeneous sizes and shapes.[195] Cu_2ZnSnS_4 NPs could be synthesized from the same reaction medium through a solvothermal process. Chloride salts were used as precursors for the metals whereas thiourea was the sulfur source. Again, PVP helped toward monodisperse NP formation.[196]

ZnS reports an exciton binding energy of 39 meV and is a promising material for use in optoelectronic devices such as light emitting diodes. PVP-coated ZnS NPs were obtained from Na_2S and $ZnSO_4$ by a simple procedure using water as solvent. These NPs could be used to fabricate ZnS-embedded PVP films by inkjet printing. The film emitted blue fluorescence from the ZnS clusters.[197] Ghosh *et al.* used PVP, thiourea, and zinc acetate for the preparation of PVP-encapsulated ZnS NPs with DMF as a solvent. The authors tuned the PVP/Zn^{2+} ratio used to optimize photoluminescence properties. A 0.007 ratio was best for nanocluster passivation, which was prerequisite for the appearance of the best possible optical properties.[198] DMF and thiourea were also employed by He *et al.* for the synthesis of ZnS (and CdS) NPs in a microwave-assisted method in the presence of PVP. The coating of the ZnS NPs by PVP caused a blue shift in its UV-Vis absorption band edge compared to bulk ZnS. The photoluminescence spectrum was broad due to emission from surface traps.[199] Finally, a simple chemical method to prepare PVP- and sodium hexametaphosphate (SHMP)-encapsulated Mn^{2+}-doped ZnS NPs by a precipitation protocol was reported using zinc acetate and $MnCl_2$. The use of PVP improved the optical properties of the NPs. Comparing the PVP- and SHMP-coated ZnS:Mn^{2+} NPs, the PVP-capped NPs displayed a higher PL intensity compared to the SHMP-capped NPs.[200]

Sub-micron tin disulfide (SnS_2) particles were synthesized via microwave irradiation for 10 min. $SnCl_4$ was used as tin precursor and thioacetamide was the sulfur source, while the solvent was a mixture of water and EG. PVP contributed in the control of morphology, preventing also the particles aggregation.[201] Tin dichloride and thioacetamide were employed as precursors for the hydrazine hydrate-assisted diethylene glycol solution synthesis of uniform near-spherical SnS NPs in the presence of PVP. This molecule acted as dispersing agent in the above process.[202] Colloidal MoS_2 NPs were prepared by solvothermal treatment of $(NH_4)_2MoS_4$ diluted in methanol with PVP as protecting molecules and $N_2H_4.H_2O$ (50%) as reducing agent. The reaction time was fixed at 3 h and the ratio of PVP to MoS_2 was tailored as a function of the preparation temperature. The obtained nanomaterials demonstrated high efficiency in catalyzing hydrogen evolution in $Ru(bpy)_3^{2+}$-based molecular systems under visible light.[203]

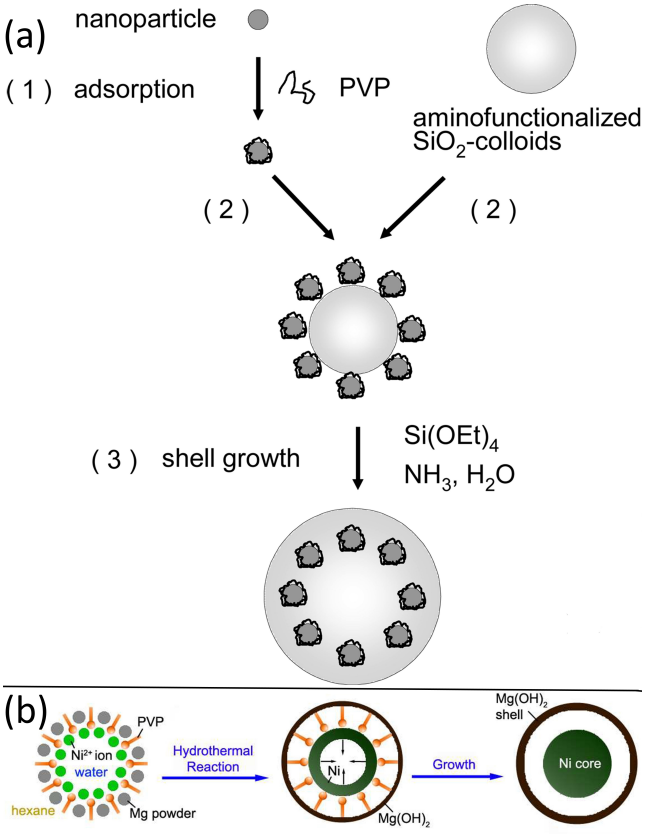

Fig. 14 (a) Diagram of the general procedure for embedding NPs in silica colloids: In the first step, PVP is adsorbed on the colloidal particles (1). After transfer in an alcohol, *e.g.* ethanol or butanol, the particles are adsorbed on amino-functionalized silica colloids, (2). Finally, after addition of ammonia, a silica shell is grown on the NP-decorated colloid by consecutive additions of tetraethoxysilane (3).[14] (b) Synthetic procedure of Ni@$Mg(OH)_2$ core-shell composite nanostructures.[212] (Figures (a) and (b) reprinted with permission from ref. 14 and 212 correspondingly)

M-Se nanostructures. CdSe NPs are model systems for the study of optical and electronic properties of quantum-confined semiconductors. PVP-coated CdSe NPs were prepared using $CdCl_2$, methanol, PVP, and Na_2SeSO_3. The PVP-capped CdSe

NPs could be dispersed in PVA solution to form PVP-CdSe-PVA films for photovoltaic applications.[204] SiO_2@CdSe/polypyrrole(PPy) composite particles could also be synthesized from SiO_2@CdSe NPs by cationic polymerization. Modification of the SiO_2 surface with PVP was necessary to deposit the CdSe NPs onto the SiO_2 cores. The PVP molecule favors a strong interaction between the core and the shell owing to its structure and partially amphiphilic property.[205] In fact, a general method to embed nanoparticles such as PVP-capped CdSe/ZnS ones in silica colloids (Fig. 14a) was reported by Graf *et al.*[14]

Silver selenide NPs were produced by a hydrothermal reaction of $AgNO_3$ with Na_2SeSO_3, PVP, and KI at 180 ^oC for 20 h. The main function of PVP was its coordination with the AgI precipitate (formed due to the presence of KI), thus generating a PVP-AgI compound which reacted with Na_2SeSO_3 to provide the final Ag_2Se product.[21] Bi_2Se_3 nanodisks and nanosheets were synthesized by Min *et al.* from Na_2SeO_3, $Bi(NO_3)_3$, PVP, EG and NH_2OH. PVP contributed to shape development and size uniformity by restricting nanodisk growth.[206] $MnSe_2$ nanorods were produced by Che and colleagues in the presence of water, DMF, PVP, $Mn(ac)_2$ and SeO_2. Here, PVP served as a soft template, depressing the growth along the [200] direction of $MnSe_2$. This templating provided control of NP size and shape.[207]

Metal telluride NPs. M-Te nanostructures have been synthesized also by wet-chemical methods, however to a lesser extent than metal sulfide and metal selenide NPs. Despite this, there are some reports of such syntheses in the presence of PVP. $Cu_{2-x}Te$ NWs were prepared by a microwave-assisted solvothermal method involving $Cu(NO_3)_2$, EG, Te nanotube templates, and $NaBH_4$, at 200 ^oC. The tellurium nanotubes were synthesized from EG, PVP and Na_2TeO_3.[208] $Cu_{2-x}Te$ micro/nanostructures with controlled shape were synthesized in air at room temperature by a simple galvanostatic electrodeposition route. Several reaction parameters were examined, such as the use of surfactants, as SDBS or CTAB, or PVP. This study suggested that copper telluride nuclei were surrounded by PVP due to weak interactions between N (from PVP molecule) and Cu. This interaction resulted in the crystallization of flower-like superstructures.[209] Furthermore, Bi_2Te_3 and its alloys are currently the most widely used thermoelectric materials for room temperature power generators or coolers. Bi_xTe_{1-x} hollow nanofibers were produced by galvanic displacement reaction of electrospun nickel nanofibers at room temperature. The Ni nanofibers were prepared by calcinating Ni-acetate/PVP NWs at 500 ^oC to form NiO nanofibers which were subsequently reduced in a H_2/N_2 mixture to form Ni nanofibers.[210]

5. Other material classes

More 'exotic' types of nanoscale materials were also prepared with PVP. Meng *et al.* reported a facile solvothermal approach to $NaYF_4$ NPs. Apart from PVP, the other reagents were YCl_3, NaF and EG. PVP could act as a chelating agent and coordinate with Y^{3+} in the process, together with its surfactant role after the formation of NPs.[211] Ni@$Mg(OH)_2$ core@shell nanocomposites were synthesized by Zhang *et al.* (Fig. 14b) using PVP, $NiCl_2$, $NH_3.H_2O$ and Mg powder in a mixture of hexane and water. The amphiphilic nature of PVP facilitated the formation of a water/hexane emulsion, generating an environment that favoured NP growth.[212] Finally, hydroxyapatite nanorods were prepared by PVP-assisted hydrothermal synthesis which yielded high aspect ratio nanorods, using $Ca(NO_3)_2$ and $(NH_4)_2HPO_4$ as starting materials. Once again, PVP was a key factor for the control of the growth direction and the uniformity.[213]

6. Summary and Outlook

This Perspective outlines the many roles PVP can adopt in chemical syntheses to high-quality nanomaterials. Through this comprehensive summary of nanomaterial syntheses, we highlight that PVP is often a suitable colloidal stabilizer, surfactant, shape-directing agent, dispersant, and even reducing agent. What roles PVP adopts depends on the specific material class, reaction conditions, and even the PVP itself on account of the many molecular weights available. As quantitative analyzed in a model Ag system, the concentration and molecular weight of PVP are critical in tuning the morphology for many types of NPs. PVP is soluble in both water and organic solvents, enabling its use with a diversity of reagents, which is a stark contrast to capping agents such as the hydrophobic oleylamine. Its solubility also renders PVP an excellent phase transfer agent while its biocompatibility is enabling application of PVP-capped nanomaterials in nanomedicine applications. Moreover, the ability of PVP to passivate surfaces of metal chalcogenide NPs minimizes defects and improves the photoluminescent properties of such materials. Still, in some cases, PVP-capping can be detrimental. For example, in certain cases PVP can block active sites for catalysis, in contrast to polyethyleneimine (PEI).[214,215,216] For this reason, PEI is sometimes considered more suitable for electrocatalytic applications compared to PVP.[217,218] As a result, effective strategies to remove surface PVP are developing to facilitate the use of shape-controlled metal NPs as catalysts and substrates for chemical sensing. This need extends beyond metals, where there are growing efforts to understand and optimize the PVP coverage of NPs to enable their use in diverse applications.

It is our intention that this Perspective serve as a comprehensive guide, presenting the beneficial and versatile roles of PVP in NP syntheses. In this way, readers will be able to reproduce the existing protocols to use PVP-capped NPs in diverse studies while at the same time designing new synthetic protocols facilely.

AUTHOR INFORMATION

Corresponding Authors

E-mails:

kkoczkur@indiana.edu (K.M.K.),
stefanos.mourdikoudis@upmc.fr (S.M.),
l.polavarapu@physik.uni-muenchen.de (L.P.),
sskrabal@indiana.edu (S.E.S.)

ACKNOWLEDGMENTS

S.E.S. acknowledges supported of Indiana University start-up funds, NSF Award CHE-1306853, and Research Corporation's Cottrell Scholar Program. S.E.S. is an Alfred P. Sloan Fellow and Camille Dreyfus Teacher-Scholar. L. P. greatly acknowledges the financial support from *Alexander von Hum-*

boldt foundation. S. M. acknowledges the facilities of the University 'Pierre et Marie Curie'.

REFERENCES

1 Y. Xia, Y. Xiong, B. Lim and S. E. Skrabalak, *Angew. Chem. Int. Ed.*, 2009, **48**, 60.

2 D. P. Chen, J. Fu and S. E. Skrabalak, *ChemNanoMat,* 2015, **1**, 18.

3 H. Ataee-Esfahani and S. E. Skrabalak, *RSC Adv.,* 2015, **5**, 47718.

4 L. Polavarapu, S. Mourdikoudis, I. Pastoriza-Santos and J. Perez-Juste, *CrystEngComm,* 2015, **17**, 3727.

5 N. Ortiz and S. E. Skrabalak, *Langmuir,* 2014, **30**, 6649.

6 S. Mourdikoudis and L. M. Liz-Marzán, *Chem. Mater.,* 2013, **25**, 1465.

7 J. Park, J. Joo, S. G. Kwon, Y. Jang and T. Hyeon, *Angew. Chem. Int. Ed.,* 2007, **46**, 2.

8 *Metal Oxide Nanoparticles in Organic Solvents*, by M. Niederberger and N. Pinna, Springer-Verlag Lodon Limited 2009

9 T. Guo, M.-S. Yao, Y.-H. Lin and C.-W. Nan, *CrystEngComm,* 2015, **17**, 3551.

10 S. V. Jadhav, D. S. Nikam, V. M. Khot, N. D. Thorat, M. R. Phadatare, R. S. Ningthoujam, A. B. Salunkhe and S. H. Pawar, *New J. Chem.,* 2013, **37**, 3121.

11 G. Lu, S. Li, Z. Guo, O. K. Farha, B. G. Hauser, X. Qi, Y. Wang, X. Wang, S. Han, X. Liu, J. S. DuChene, H. Zhang, Q. Zhang, X. Chen, J. Ma, S. C. J. Loo, W. D. Wei, Y. Yang, J. T. Hupp and F. Huo, *Nat. Chem.,* 2012, **4**, 310.

12 H. Ziaei-Azad and N. Semagina, *Appl. Catal. A-Gen.,* 2014, **482**, 327.

13 *Synthesis of Noble Metal Nanoparticles* (Ph.D. Thesis by M. Bahadory), 2008, Drexler University, USA.

14 C. Graf, S. Dembski, A. Hofmann and E. Ruhl, *Langmuir,* 2006, **22**, 5604.

15 R. Si, Y.-W. Zhang, L.-P. You and C.-H. Yan, *J. Phys. Chem. B,* 2006, **110**, 5994.

16 A. Kyrychenko, O. M. Korsun, I. I. Gabin, S. M. Kovalenko and O. N. Kalugin, *J. Phys. Chem. C,* 2015, **119**, 7888.

17 X. Wu, Y. Zhao, C. Yang and G. He, *J. Mater. Sci.,* 2015, **50**, 4250.

18 W. A. Saidi, H. Feng and K. A. Fichthorn, *J. Phys. Chem. C,* 2013, **117**, 1163.

19 Y. Xiong, H. Cai, B. J. Wiley, J. Wang, M. J. Kim and Y. Xia, *J. Am. Chem.,* 2007, **129**, 3665.

20 A. Kedia and P. S. Kumar, *J. Phys. Chem. C,* 2012, **116**, 23721.

21 H. Liu, B. Zhang, H. Shi, Y. Tang, K. Jiao and X. Fu, *J. Mater. Chem.,* 2008, **18**, 2573.

22 Y. Gao, P. Jiang, D. F. Liu, H. J. Yuan, X. Q. Yan, Z. P. Zhou, J. X. Wang, L. Song, L. F. Liu, W. Y. Zhou, G. Wang, C. Y. Wang, S. S. Xie, J. M. Zhang and D. Y. Shen, *J. Phys. Chem. B,* 2004, **108**, 12877.

23 R.-Z. Li, A. Hu, D. Bridges, T. Zhang, K. D. Oakes, R. Peng, U. Tumuluri, Z. Wu and Z. Feng, *Nanoscale,* 2015, **7**, 7368.

24 L. Polavarapu, K. K. Manga, H. D. Cao, K. P. Loh and Q.-H. Xu, *Chem. Mater.,* 2011, **23**, 3273.

25 *Mesoscopic organization and properties of nanocrystal of metals, metal oxides and other materials*, Ph.D. thesis by P. J. Thomas, Jawaharlar Nehru Centre for Advanced Scientific Research (Deemed University), 2003, Bangalore, India.

26 S. Guo, S. Dong and E. Wang, *ACS Nano,* 2010, **4**, 547.

27 X. M. Zeng, G. P. Martin and C. Marriott, *Int. J. Pharm.,* 2001, **218**, 63.

28 Y. Sun and Y. Xia, *Adv. Mater.,* 2002, **14**, 833.

29 M. Giersig, I. Pastoriza-Santos and L. M. Liz-Marzán, *J. Mater. Chem.*, 2004, **14**, 607.

30 Y. Wang, D. Wan, S. Xie, X. Xia, C. Z. Huang and Y. Xia, *ACS Nano*, 2013, **7**, 4586.

31 F. Kim, S. Connor, H. Song, T. Kuykendall and P. Yang, *Angew. Chem. Int. Ed.*, 2004, **43**, 3673.

32 M-C. Daniel and D. Astruc, *Chem. Rev.*, 2004, **104**, 293.

33 E. C. Dreaden, A. M. Alkilany, X. Huang, C. J. Murphy and M. A. El-Sayed, *Chem. Soc. Rev.*, 2012, **41**, 2740.

34 Y. Wang, P. Chen and M. Liu, *Nanotechnology*, 2006, **17**, 6000.

35 Q. Shen, Q. Min, J. Shi, L. Jiang, J-R. Zhang, W. Hou and J-J. Zhu, *J. Phys. Chem. C*, 2009, **113**, 1267.

36 Y. Wang, S. Xie, J. Liu, J. Park, C. Z. Huang and Y. Xia, *Nano Lett.*, 2013, **13**, 2276.

37 N. Fan, Y. Yang, W. Wang, L. Zhang, W. Chen, C. Zou and S. Huang, *ACS Nano*, 2013, **6**, 4072.

38 F. Ye, W. Hu, T. Zhang, J. Yang and Y. Ding, *Electrochim. Acta*, 2012, **83**, 383.

39 Y-J. Zhang, Q. Yao, Y. Zhang, T-Y. Cui, D. Li, W. Liu, W. Lawrence and Z-D. Zhang, *Cryst. Growth Des.*, 2008, **8**, 3206.

40 W. Zhou, L. Lin, D. Zhao and L. Guo, *J. Am. Chem. Soc.*, 2011, **133**, 8389.

41 S. K. Singh, M. Yadav, S. Behrens and P. W. Roesky, *Dalton Trans.*, 2013, **42**, 10404.

42 A. Villa, D. Wang, D. S. Su and L. Prati, *Catal. Sci. Technol.*, 2015, **5**, 55.

43 J-J. Lv, J-N. Zheng, S-S. Li, L-L. Chen, A-J. Wang and J-J. Feng, *J. Mater. Chem. A*, 2014, **2**, 4384.

44 H. Zhang, M. Jin and Y. Xia, *Chem. Soc. Rev.,* 2012, **41**, 8035.

45 H. H. Huang, X. P. Ni, G. L. Loy, C. H. Chew, K. L. Tan, F. C. Loh, J. F. Deng and G. Q. Xu, *Langmuir*, 1996, **12**, 909.

46 B. Yin, H. Ma, S. Wang and S. Chen, *J. Phys. Chem. B*, 2003, **107**, 8898.

47 W. A. Al-Saidi, H. Feng and K. A. Fichthorn, *Nano Lett.*, 2012, **12**, 997.

48 Y. Sun and Y. Xia, *Science*, 2002, **298**, 2176.

49 A. R. Tao, S. Habas and P. Yang, *Small*, 2008, **4**, 310.

50 C. N. R. Rao, H. S. S. R. Matte, R. Voggu and A. Govindaraj, *Dalton Trans.*, 2012, **41**, 5089.

51 S. Selvam and M. Sundrarajan, *Carbohyd. Pol.*, 2012, **87**, 1419.

52 A. Panáček, L. Kvítek, R. Prucek, M. Kolář, R. Večeřová, N. Pizúrová, V. K. Sharma, T. Nevěčná and R. Zbořil, *J. Phys. Chem. B*, 2006, **110**, 16248.

53 S. Sarina, E. R. Waclawik and H. Zhu, *Green Chem.,* 2015, **15**, 1814.

54 M. Fan and A. G. Brolo, *Phys. Chem. Chem. Phys.*, 2009, **11**, 7381.

55 M. J. Mulvihill, X. Y. Ling, J. Henzie and P. Yang, *J. Am. Chem. Soc.*, 2010, **132**, 268.

56 X. Xia, J. Zeng, L. K. Oetjen, Q. Li and Y. Xia, *J. Am. Chem. Soc.*, 2012, **134**, 1793.

57 A. Tao, P. Sinsermsuksakul and P. Yang, *Angew. Chem. Int. Ed.*, 2006, **45**, 4597.

58 Y. Xia, X. Xia and H-C. Peng, *J. Am. Chem. Soc.*, 2015, **137**, 7947.

59 Y. Sun, B. Gates, B. Mayers and Y. Xia, *Nano Lett.,* 2002, **2**, 165.

60 Y. Sun, Y. Yin, B. T. Mayers, T. Herricks and Y. Xia, *Chem. Mater.*, 2002, **14**, 4736.

61 K. K. Caswell, C. M. Bender and C. J. Murphy, *Nano Lett.*, 2003, **3**, 667.

62 Y. Sun, B. Mayers, T. Herricks and Y. Xia, *Nano Lett.*, 2003, **3**, 955.

63 A. Tao, F. Kim, C. Hess, J. Goldberger, R. He, Y. Sun, Y. Xia and P. Yang, *Nano Lett.,* 2003, **3**, 1229.

64 P. Jiang, S-Y. Li, S-S. Xie, Y. Gao and L. Song, *Chem. Eur. J.*, 2004, **10**, 4817.

65 S. Coskun, B. Aksoy and H. E. Unalan, *Cryst. Growth Des.*, 2011, **11**, 4963.

66 M. Tsuji, X. Tang, M. Matsunaga, Y. Maeda and M. Watanabe, *Cryst. Growth Des.*, 2010, **10**, 5238.

67 B. Wiley, Y. Sun and Y. Xia, *Acc. Chem. Res.,* 2007, **40**, 1067.

68 B. J. Wiley, Z. Wang, J. Wei, Y. Yin, D. H. Cobden and Y. Xia, *Nano Lett.,* 2006, **6**, 2273.

69 Y. Sun, *Chem. Soc. Rev.,* 2013, **42**, 2497.

70 M. Faraday, *Philos. Trans. R. Soc. London*, 1857, **147**, 145.

71 J. Turkevich, P. C. Stevenson and J. Hillier, *Discuss. Faraday Soc.*, 1951, **11**, 55.

72 M. Brust, M. Walker, D. Bethell, D. J. Schiffrin and R. Whyman, *J. Chem. Soc., Chem. Commun.,* 1994, 801.

73 C. L. Nehl, H. Liao and J. H. Hafner, *Nano Lett.,* 2006, **6**, 683.

74 M. Haruta, *J. New. Mat. Electrochem. Systems*, 2004, **7**, 163.

75 M. Rocha, C. Fernandes, C. Pereira, S. L. H. Rebelo, M. F. R. Pereira and C. Freire, *RSC Adv.*, 2015, **5**, 5131.

76 S-H. Liu, W. A. Saidi, Y. Zhou and K. A. Fichthorn, *J. Phys. Chem. C,* 2015, **119**, 11982.

77 S. Guo and E. Wang, *Inorg. Chem.*, 2007, **46**, 6740.

78 E. Carbó-Argibay, B. Rodríguez-González, J. Pacifico, I. Pastoriza-Santos, J. Pérez-Juste and L. M. Liz-Marzán, *Angew. Chem. Int. Ed.,* 2007, **46**, 8983.

79 I. Pastoriza-Santos and L. M. Liz-Marzán, *Adv. Funct. Mater.*, 2009, **19**, 679.

80 Y. Chen, X. Gu, C-G. Nie, Z-Y. Jiang, Z-X. Xie and C-J. Lin, *Chem. Commun.,* 2005, 4181.

81 S. Barbosa, A. Agrawal, L. Rodríguez-Lorenzo, I. Pastoriza-Santos, R. A. Alvarez-Puebla, A. Kornowski, H. Weller and L. M. Liz-Marzán, *Langmuir*, 2010, **26**, 14943.

82 P. S. Kumar, I. Pastoriza-Santos, B. Rodríguez-González, F. J. García de Adajo and L. M. Liz-Marzán, *Nanotechnology*, 2008, **19**, 015606.

83 M. Thiemann, E. Scheibler and K. W. Wiegand, *Ullmann's Encyclopedia of Industrial Chemistry*, Wiley-VCH, 2000, **24**, 177.

84 X. Yu and P. G. Pickup, *J. Power Sources*, 2008, **182**, 124.

85 K. Jiang, H-X. Zhang, S. Zou and W-B Cai, *Phys. Chem. Chem. Phys.* 2014, **16**, 20360.

86 V. Mazumder and S. Sun, *J. Am. Chem. Soc.*, 2009, **131**, 4588.

87 S-W Kim, M. Kim, W. Y. Lee and T. Hyeon, *J. Am. Chem. Soc.*, 2002, **124**, 7642.

88 E. Formo, E. Lee, D. Campbell and Y. Xia, *Nano Lett.*, 2008, **8**, 668.

89 T. S. Ahmadi, Z. L. Wang, T. C. Green, A. Henglein and M. A. El-Sayed, *Science*, 1996, **272**, 1924.

90 R. Narayanan and M. A. El-Sayed, *Nano Lett.,* 2004, **4**, 1343.

91 J. Chen, T. Herricks, M. Geissler and Y. Xia, *J. Am. Chem. Soc.*, 2004, **126**, 10854.

92 Y. Xiong, B. Wiley, J. Chen, Z-Y. Li, Y. Yin and Y. Xia, *Angew. Chem. Int. Ed.*, 2005, **44**, 7913.

93 H. Song, F. Kim, S. Connor, G. A. Somorjai and P. Yang, *J. Phys. Chem. B*, 2005, **109**, 188.

94 Y. Borodko, S. F. Habas, M. Koebel, P. Yang, H. Frei and G. A. Somorjai, *J. Phys. Chem. B*, 2006, **110**, 23052.

95 X. Huang and N. Zheng, *J. Am. Chem. Soc.*, 2009, **131**, 4602.

96 I. Washio, Y. Xiong, Y. Yin and Y. Xia, *Adv. Mater.,* 2006, **18**, 1745.

97 M. Crespo-Quesada, A. Yarulin, M. Jin, Y. Xia and L. Kiwi-Minsker, *J. Am. Chem. Soc.*, 2011, **133**, 12787.

98 B. Lim, M. Jiang, J. Tao, P. H. C. Camargo, Y. Zhu and Y. Xia, *Adv. Funct. Mater.,* 2009, **19**, 189.

99 N. Su, X. Chen, Y. Ren, B. Yue, H. Wang, W. Cai and H. He, *Chem. Commun.,* 2015, **51**, 7195.

100 J. Yin, J. Wang, M. Li, C. Jin and T. Zhang, *Chem. Mater.,* 2012, **24**, 2645.

101 S. J. Kweskin, R. M. Rioux, H. Song, K. Komvopoulos, P. Yang and G. A. Somorjai, *ACS Catal.*, 2012, **2**, 2377.

102 F. Novio, K. Philippot and B. Chaudret, *Catal. Lett.,* 2010, **140**, 1.

103 T. Ayvali, P. Lecante, P.-F. Fazzini, A. Gillet, K. Philippot and B. Chaudret, *Chem. Commun.*, 2014, **50**, 10809.

104 H-l. Liu, F. Nosheen and X. Wang, *Chem. Soc. Rev.*, 2015, **44**, 3056.

105 M. Tsuji, R. Matsuo, P. Jiang, N. Miyamae, D. Ueyama, M. Nishio, S. Hikino, H. Kumagae, K. S. N. Kamarudin and X-L. Tang, *Cryst. Growth. Des.*, 2008, **8**, 2528.

106 Y-J. Wang, N. Zhao, B. Fang, H. Li, X. T. Bi and H. Wang, *Chem. Rev.*, 2015, **115**, 3433.

107 J. Sun, J. Wang, Y. Zhang, P. Wan, L. Luo, F. Wang and X. Sun, *Dalton Trans.*, 2014, **43**, 12495.

108 D. S. Kilin, O. V. Prezhdo and Y. Xia, *Chem. Phys. Lett.,* 2008, **458**, 113.

109 S. Mourdikoudis, M. Chirea, D. Zanaga, T. Altantzis, M. Mitrakas, S. Bals, L. M. Liz-Marzán, J. Perez-Juste and I. Pastoriza-Santos, *Nanoscale*, 2015, **7**, 8739.

110 N. V. Long, M. Ohtaki, T. Matsubara, M. T. Cao and M. Nogami, *J. Phys. Chem. C*, 2012, **116**, 12265.

111 B. Lim, J. Wang, P. H. C. Camargo, M. Jiang, M. J. Kim and Y. Xia, *Nano Lett.,* 2008, **8**, 2535.

112 H. Zhang, M. Jin, H. Liu, J. Wang, M. J. Kim, D. Yang, Z. Xie, J. Liu and Y. Xia, *ACS Nano*, 2011, **5**, 8212.

113 B. Lim, J. Wang, P. H. C. Camargo, C. M. Cobley, M. J. Kim and Y. Xia, *Angew. Chem. Int. Ed.*, 2009, **48**, 6304.

114 Y. Wu, S. Cai, D. Wang, W. He and Y. Li, *J. Am. Chem. Soc.*, 2012, **134**, 8975.

115 X. Huang, Y. Li, Y. Li, H. Zhou, X. Duan and Y. Huang, *Nano Lett.,* 2012, **12**, 4265.

116 L. Polavarapu, J. Perez-Juste, Q.-H. Xu and L. M. Liz-Marzán, *J. Mater. Chem. C,* 2014, **2**, 7460.

117 L. Polavarapu and L. M. Liz-Marzán, *Phys. Chem. Chem. Phys.,* 2013, **15**, 5288.

118 W. Lewandowski, M. Fruhnert, J. Mieczkowski, C. Rockstuhl and E. Gorecka, *Nat. Commun.,* 2015, **6**:6590

119 J. Dintinger, S. Mühlig, C. Rockstuhl and T. Scharf, *Opt. Mater. Express,* 2012, **2**, 269.

120 G. Zheng, K. Kaefer, S. Mourdikoudis, L. Polavarapu, B. Vaz, S. E. Cartmell, A. Bouleghlimat, N. J. Buurma, L. Yate, Á. R. de Lera, L. M. Liz-Marzán, I. Pastoriza-Santos and J. Pérez-Juste, *J. Phys. Chem. Lett.*, 2015, **6**, 230.

121 L. Polavarapu, A. La Porta, S. M. Novikov, M. Coronado-Puchau and L. M. Liz-Marzán, *Small*, 2014, **10**, 3065.

122 A. Tao, P. Sinsermsuksakul and P. Yang, *Nat. Nanotech.*, 2007, **2**, 435.

123 A. R. Tao, J. Huang and P. Yang, *Accounts Chem. Res.*, 2008, **41**, 1662.

124 Y. H. Lee, C. K. Lee, B. Tan, J. M. Rui Tan, I. Y. Phang and X. Y. Ling, *Nanoscale*, 2013, **5**, 6404.

125 C. Fernández-López, L. Polavarapu, D. M. Solís, J. M. Taboada, F. Obelleiro, R. Contreras-Cáceres, I. Pastoriza-Santos and J. Pérez-Juste, *ACS Appl. Mater. Interfaces*, 2015, **7**, 12530.

126 M. Mulvihill, A. Tao, K. Benjauthrit, J. Arnold and P. Yang, *Angew. Chem. Int. Ed.*, 2008, **47**, 6456.

127 C. Graf, D. L. J. Vossen, A. Imhof and A. van Blaaderen, *Langmuir*, 2003, **19**, 6693.

128 A. Guerrero-Martínez, J. Pérez-Juste and L. M. Liz-Marzán, *Adv. Mater.*, 2010, **22**, 1182.

129 A. Vanderkooy and M. A. Brook, *ACS Appl. Mater. Interfaces,* 2012, **4**, 3980.

130 Z. Niu and Y. Li, *Chem. Mater.*, 2014, **26**, 72.

131 C. H. Moran, M. Rycenga, Q. Zhang and Y. Xia, *J. Phys. Chem. C*, 2011, **115**, 21852.

132 L. Rodríguez-Lorenzo, R. A. Álvarez-Puebla, I. Pastoriza-Santos, S. Mazzucco, O. Stéphan, M. Kociak, L. M. Liz-Marzán and F. J. García de Abajo, *J. Am. Chem. Soc.,* 2009, **131**, 4616.

133 N. Long, M. Ohtaki, M. Nogami and T. Hien, *Colloid Polym. Sci.*, 2011, **289**, 1373.

134 J. Monzó, M. T. M. Koper and P. Rodriguez, *ChemPhysChem*, 2012, **13**, 709.

135 M. Luo, Y. Hong, W. Yao, C. Huang, Q. Xu and Q. Wu, *J. Mater. Chem. A*, 2015, **3**, 2770.

136 T. Tokuno, M. Nogi, M. Karakawa, J. Jiu, T. Nge, Y. Aso and K. Suganuma, *Nano Res.*, 2011, **4**, 1215.

137 L. Hu, H. S. Kim, J.-Y. Lee, P. Peumans and Y. Cui, *ACS Nano,* 2010, **4**, 2955.

138 A. M. Reddy, B. K. Kwak, H. J. Shim, C. Ahn, S. H. Cho, B. J. Kim, S. Y. Jeong, S.-J. Hwang and S. H. Yuk, *Contrast Media Mol. Imag.,* 2009, **4**, 118.

139 J. Wang, G. Tang, Y. Qian, *Appl. Phys. A,* 2007, **86**, 261.

140 Y. Zhang, J.-Y. Liu, S. Ma, Y.-J. Zhang, X. Zhao, X.-D. Zhang and Z.-D. Zhang, *J. Mater. Sci.-Mater. Med.,* 2010, **21**, 1205.

141 X.-M. Liu and J.-K. Kim, *Mater. Lett.,* 2009, **63**, 428.

142 J. Zhang, J. Chen and Z. Wang, *Mater. Lett.,* 2007, **61**, 1629.

143 X. Lu, M. Niu, R. Qiao and M. Gao, *J. Phys. Chem. B,* 2008, **112**, 14390.

144 H.-Y. Lee, S.-H. Lee, C. Xu, J. Xie, J.-H. Lee, B. Wu, A. L. Koh, X. Wang, R. Sinclair, S. X. Wang, D. G. Nishimura, S. Biswal, S. Sun, S. H. Cho and X. Chen, *Nanotechnology,* 2008, **19**, 165101.

145 Y. Hou, J. Yu and S. Gao, *J. Mater. Chem.,* 2003, **13**, 1983.

146 H.-L. Liu, S. P. Ko, J.-H. Wu, M.-H. Jung, J. H. Min, J. H. Lee, B. H. An and Y. K. Kim, *J. Magn. Magn. Mater.,* 2007, **310**, e815.

147 K. Tao, S. Song, J. Ding, H. Dou and K. Sun, *Colloid. Polym. Sci.,* 2011, **289**, 361.

148 Y. Zheng, Y. Cheng, Y. Wang, F. Bao, L. Zhou, X. Wei, Y. Zhang and Q. Zheng, J. *Phys. Chem. B*, 2006, **110**, 3093.

149 C.-L. Fang, K. Qian, J. Zhu, S. Wang, X. Lv and S.-H. Yu, *Nanotechnology*, 2008, **19**, 125601.

150 M. Sivakumar, S. Kanagesan, V. Umapathy, R. S. Babu and S. Nithiyanantham, *J. Supercond. Nov. Magn.*, 2013, **26**, 725.

151 U. Kurtan, R. Topkaya and A. Baykal, *Mater. Res. Bull.*, 2013, **48**, 4889.

152 C. Mateo-Mateo, C. Vazquez-Vazquez, M. C. Bujan-Nunez, M. A. Lopez-Quintela, D. Serantes, D. Baldomir and J. Rivas, *J. Non-Cryst. Solids*, 2008, **354**, 5236.

153 Q. Liu, L. Lai, X. Fu, F. Zhu, J. Sun, H. Rong, M. He, Q. Chen and Z. Xu, *J. Mater. Sci.*, 2007, **42**, 10113.

154 Y. Tang, X. Wang, Q. Zhang, Y. Li and H. Wang, *Synthet. Met.*, 2012, **162**, 309.

155 S. Xian, F. Wang, Y.-X. J. Wang, J. C. Yu and K. C.-F. Leung, *J. Mater. Chem.*, 2010, **20**, 5086.

156 P. Sivakumar, R. Ramesh, A. Ramanand, S. Ponnusamy and C. Muthamilchelvan, *AIP Conf. Proc.*, 2011, **1347**, 297.

157 R. Topkaya, U. Kurtan, A. Baykal and M. S. Toprak, *Ceram. Int.*, 2013, **39**, 5651.

158 Y.-D. Luo, Y.-H. Lin, Y.-N. Feng, Y.-J. Zhang, Y. Song, Y. Shen and C.-W Nan, *J. Appl. Phys.*, 2012, **112**, 116101.

159 R. Shi, G. Chen, W. Ma, D. Zhang, G. Qiu and X. Liu, *Dalton Trans.*, 2012, **41**, 5981.

160 A. Baykal, M. Bitrak, B. Unal, H. Kavas, Z. Durmus, S. Ozden and M. S. Toprak, *J. Alloy. Compd.*, 2010, **502**, 199.

161 S. F. Wei, J. S. Lian and Q. Jiang, *Appl. Surf. Sci.*, 2009, **255**, 6978.

162 R. Hariharan, S. Senthilkumar, A. Suganthi and M. Rajarajan, *J. Photoch. Photobio. A.*, 2013, **252**, 107.

163 K. Raja, P. S. Ramesh and D. Geetha, *Spectrochim. Acta A*, 2014, **120**, 19.

164 X. Wang, Z. Pang, M. Wu, X. Lu, G. Li, Z. Sun and L. Zhang, *Micro. Nano. Lett*., 2012, **7**, 523.

165 J. Wang, T. Tsuzuki, B. Tang, P. Cizek, L. Sun and X. Wang, *Colloid Polym. Sci*., 2010, **288**, 1705.

166 Y. Yuliah and A. Bahtiar, *AIP Conf. Proc*., 2013, **1554**, 139.

167 G. Shan, H. Hao, X. Wang, Z. Shang, Y. Chen and Y. Liu, *Colloids Surf. A*, 2012, **405**, 1.

168 D. Archana, B. K. Singh, J. Dutta and P. K. Dutta, *Carbohyd. Pol*., 2013, **95**, 530.

169 J. S. Chen, J. Liu, S. Z. Qiao, R. Xu and X. W. D. Lou, *Chem. Commun*., 2011, **47**, 10443.

170 L. Saravanan, R. M. Kumar, A. Pandurangan and R. Jayavel, *Optoelectron. Adv. Mat*., 2010, **4**, 1676.

171 C. Liu, W. Sun, Y. Zhuo, C. Liu and Y. Chu, *J. Alloy Compd*., 2013, **581**, 115.

172 H. Zhang, X. Ren and Z. Chi, *J. Cryst. Growth*, 2007, **304**, 206.

173 S. Wu, T. Liu, W. Zeng, J. He, W. Yu and Z. Gou, *J. Mater. Sci.-Mater. El*., 2013, **24**, 2404.

174 J. C. Park, J. Kim, H. Kwon and H. Song, *Adv. Mater*., 2009, **21**, 803.

175 M. H. Kim, B. Lim, E. P. Lee and Y. Xia, *J. Mater. Chem*., 2008, **18**, 4069.

176 P. Liu, Z. Li, W. Cai, M. Fang and X. Luo. *RSC Adv*., 2011, **1**, 847.

177 X. Han, M. Jin, S. Xie, Q. Kuang, Z. Jiang, Y. Jiang, Z. Xie and L. Zheng, *Angew. Chem. Int. Ed*., 2009, **48**, 9180.

178 W. Wu, X. Zou, Q. Li, B. Liu, B. Liu, R. Liu, D. Liu, Z. Li, W. Cui, Z. Liu, D. Li, T. Cui and G. Zou, *J. Nanomater*., 2011, **2011**, 841701.

179 Z. Yang, D. Han, D. Ma, H. Liang, L. Liu and Y. Yang, *Cryst. Growth Des*., 2010, **10**, 291.

180 T. Itoh, T. Uchida, N. Izu, I. Matsubara and W. Shin, *Materials,* 2013, **6**, 2119.

181 S. Phoka, P. Laokul, E. Swatsitang, V. Promarak, S. Seraphin and S. Maensiri, *Mater. Chem. Phys*., 2009, **115**, 423.

182 S. Phoka, S. Pinitsoontorn, P. Chirawatkul, Y. Poo-arporn and S. Maensiri, *Nanoscale Res. Lett*., 2012, **7**, 425.

183 Y. Cui, X. Lai, L. Li, Z. Hu, S. Wang, J. E. Halpert, R. Yu and D. Wang, *ChemPhysChem,* 2012, **13**, 2610.

184 Q. Xia, X. Chen, K. Zhao and J. Liu, *Mater. Chem. Phys*., 2008, **111**, 98.

185 M. Pattabi, B. S. Amma, K. Manzoor and G. Sanjeev, *Sol. Energ. Mat. Sol. C,* 2007, **91**, 1403.

186 M. Pattabi, B. S. Amma and K. Manzoor, *Mater. Res. Bull*., 2007, **42**, 828.

187 L. Saravanan, S. Diwakar, R. Mohankumar, A. Pandurangan and R. Jayavel, *Nanomater. Nanotechnol*., 2011, **1**, 42.

188 W. Qingqing, Z. Gaoling and H. Gaorong, *Mater. Lett*., 2005, **59**, 2625.

189 A. W. Schill and M. A El-Sayed, *J. Phys. Chem. B,* 2004, **108**, 13619.

190 N. Soltani, E. Saion, W. M. M. Yunus, M. Navasery, G. Bahmanrokh, M. Erfani, M. R. Zare and E. Gharibshahi, *Sol. Energy,* 2013, **97**, 147.

191 Z. Qin, H. Sun, Z. Jiang, X. Jiao and D. Chen, *CrystEngComm,* 2013, **15**, 897.

192 H. Qi, J-F. Huang, L.-Y. Cao, J.-P. Wu and D.-Q. Wang, *Ceram. Int*., 2012, **38**, 2195.

193 Z. Fang, C. Wang, F. Fan, S. Hao, L. Long, Y. Song and T. Qiang, *Chin. J. Chem*., 2013, **31**, 1015.

194 X. Yan, E. Michael, S. Komarneni, J. R. Brownson and Z.-F. Yan, *Ceram. Int*., 2013, **39**, 4757.

195 M. Cao, C. Li, B. Zhang, J. Huang, L. Wang and Y. Shen, *J. Alloy Compd*., 2015, **622**, 695.

196 S. S. Mali, H. Kim, C. S. Shim, P. S. Patil and C. K. Hong, *Phys. Status Solidi-R*., 2013, **7**, 1050.

197 S. Ummartyotin, N. Bunnak, J. Juntaro, M. Sain and H. Manuspiya, *C. R. Phys*., 2012, **13**, 994.

198 G. Ghosh, M. K. Naskar, A. Patra and M. Chatterjee, *Opt. Mater*., 2006, **28**, 1047.

199 R. He, X.-f. Qian, J. Yin, H.-a. Xi, L.-j. Bian and Z.-k. Zhu, *Colloids Surf. A,* 2003, **220**, 151.

200 G. Murugadoss, *J. Lumin*. 2010, **130**, 2207.

201 H. Yang, C. Huang and X. Su, *Mater. Lett*., 2006, **60**, 3714.

202 L. Ren, Z. Jin, S. Cai, J. Yang and Z. Hong, *Cryst. Res. Technol*., 2012, **47**, 461.

203 X. Zong, Y. Na, F. Wen, G. Ma, J. Yang, D. Wang, Y. Ma, M. Wang, L. Su and C. Li, *Chem. Commun*., 2009, 4536.

204 W. E. Mahmoud and H. M. El-Mallah, *J. Phys. D: Appl. Phys*., 2009, **42**, 035502.

205 L. Hao, X. Gong, S. Xuan, H. Zhang, X. Gong, W. Jiang and Z. Chen, *Appl. Surf. Sci*., 2006, **252**, 8724.

206 Y. Min, G. D. Moon, B. S. Kim, B. Lim, J.-S. Kim, C. Y. Kang and U. Jeong, *J. Am. Chem. Soc*., 2012, **134**, 2872.

207 J. Zhang, J. Liu, C. Liang, F. Zhang and R. Che, *J. Alloy Compd.,* 2013, **548**, 13.

208 G.-H. Dong, Y.-J. Zhu, G.-F. Cheng and Y.-J. Ruan, *Mater. Lett.,* 2012, **76**, 69.

209 Y. Ni, H. Zhang, J. Xi, X. Wang, Y. Zhang, Y. Xiao, X. Ma and J. Hong, *CrystEngComm,* 2014, **16**, 7869.

210 K.-J. Lee, H. Song, Y.-I. Lee, H. Jung, M. Zhang, Y.-H. Choa and N. V. Myung, *Chem. Commun.,* 2011, **47**, 9107.

211 F. Meng, S. Liu, Y. Wang, C. Tao, P. Xu, W. Guo, L. Shen, X. Zhang and S. Ruan, *J. Mater. Chem.,* 2012, **22**, 22382.

212 M. Zhang, W. Song, Q. Chen, B. Miao and W. He, *ACS Appl. Mater. Interfaces,* 2015, **7**, 1533.

213 A. J. Nathanael, Y. H. Seo and T. H. Oh, *J. Nanomater.,* 2015, **2015**, 621785.

214 H. Lee, S. E. Habas, S. Kweskin, D. Butcher, G. A. Somorjai and P. Yang, *Angew. Chem. Int. Ed.*, 2006, **45**, 7824.

215 L. Bai, H. Zhu, J. S. Thrasher and S. C. Street, *ACS Appl. Mater. Interfaces,* 2009, **1**, 2304.

216 P. L. Cuo, W. F. Chen, H. Y. Huang, I. C. Chang and S. A. Dai, *J. Phys. Chem. B*, 2006, **110**, 3071.

217 Z. Q. Tian, S. P. Jiang, Z. Liu and L. Li, *Electrochem. Commun.,* 2007, **9**, 1613.

218 H. P. Liang, T. G. J. Jones, N. S. Lawrence, L. Jiang and J. S. J. Barnard, *J. Phys. Chem. C*, 2008, **112**, 4327.